Automated Micromanipulation of Micro Objects

by

Mohsen Shahini

A thesis

presented to the University of Waterloo

in fulfillment of the

thesis requirement for the degree of

Doctor of Philosophy

in

Mechanical Engineering

Waterloo, Ontario, Canada, 2011

AUTHOR'S DECLARATION

I hereby declare that I am the sole author of this thesis. This is a true copy of the thesis, including any required final revisions, as accepted by my examiners.

I understand that my thesis may be made electronically available to the public.

Abstract

In recent years, research efforts in the development of Micro Electro Mechanical Systems, (MEMS) including microactuators and micromanipulators, have attracted a great deal of attention. The development of microfabrication techniques has resulted in substantial progress in the miniaturization of devices such as electronic circuits. However, the research in MEMS still lags behind in terms of the development of reliable tools for post-fabrication processes and the precise and dexterous manipulation of individual micro size objects.

Current micromanipulation mechanisms are prone to high costs, a large footprint, and poor dexterity and are labour intensive. To overcome such, the research in this thesis is focused on the utilization of microactuators in micromanipulation. Microactuators are compliant structures. They undergo substantial deflection during micromanipulation due to the considerable surface micro forces. Their dominance in governing micromanipulation is so compelling that their effects should be considered in designing microactuators and microsensors.

In this thesis, the characterization of the surface micro forces and automated micromanipulation are investigated. An inexpensive experimental setup is proposed as a platform to replace Atomic Force Microscopy (AFM) for analyzing the force characterization of micro scale components. The relationship between the magnitudes of the surface micro forces and the parameters such as the velocity of the pushing process, relative humidity, temperature, hydrophilicity of the substrate, and surface area are empirically examined.

In addition, a precision automated micromanipulation system is realized. A class of artificial neural networks (NN) is devised to estimate the unmodelled micro forces during the controlled pushing of micro size object along a desired path. Then, a nonlinear controller is developed for the controlled pushing of the micro objects to guarantee the stability of the closed loop system in the Lyapunov sense. To validate the performance of the proposed controller, an experimental setup is designed.

The application of the proposed controller is extended to precisely push several micro objects, each with different characteristics in terms of the surface micro forces governing the manipulation process. The proposed adaptive controller is capable of learning to adjust its weights effectively when the surface micro forces change under varying conditions. By using the controller, a fully automated sequential positioning of three micro objects on a flat substrate is performed. The results are compared with those of the identical sequential pushing by using a conventional linear controller.

The results suggest that artificial NNs are a promising tool for the design of adaptive controllers to accurately perform the automated manipulation of multiple objects in the microscopic scale for microassembly.

Acknowledgements

In order to complete this thesis, I was very fortunate to have received the kind support from my teachers, family, and friends. Their words of encouragements have had a remarkable impact on my growth and development.

First and foremost, I would like to thank my supervisors, Professor William Melek and Professor John Yeow for their supervision and encouragement throughout my research. I would also like to acknowledge my oral examination committees, Professor John Medley, Professor Patricia Neiva, Professor Eihab Abdel-Rahman, and Prof Alireza Sadeghian for dedicating their time to the examination committee, as well as the valuable feedback they have contributed.

I have been fortunate to have worked with a talented group in the Advanced Micro/Nano Devices lab. It was through their companionship that I was able to overcome the challenges and obstacles that is the nature of research. I thank them all.

While in university, I have had the opportunity to share and learn from a group of great friends. I was able to receive inspiration, energy, and advice from each of them, which allowed me to look at life from a new angle. Olivier Nguon, Arash Tajik, Mike Silagadze, Remi Gagnon, Hamidreza Alemohammad, Yelda Turkan, Derya Demirtas, Azad Ghazizadeh, Jonathan Juger, Pedram Hassanzadeh, Sara Matthews, Sara Sadri, and Babak Ebrahimi are just a few of these friends that I wish to express my appreciation to.

Finally, I owe my deepest gratitude to my parents, Masoumeh and Mohammad, my sisters, Malihe and Motahare, my brother, Mehdi, and my partner Linda. I am indebted to the love, sacrifices and encouragement that they have provided continuously.

Dedication

To those who seek the scientific truth, and continuous expansion of human society's collective knowledge.

Table of Contents

List of Figures

List of Tables

Nomenclature

Nomenclature	Description
$F(x_1, \dots, x_p)$	Function of p parameters
v_{ss}	Scale speed of an object
V_{actual}	Actual speed of an object
$\emptyset$	Vector of the environmental parameters
R_{ms}	Surface roughness in the micro scale
R_a	Surface roughness in the macro scale
RH	Relative humidity
T	Temperature
E_s , E_o	Young's modulus
v_s v_o	Poisson ratio
m	Mass
A	Surface area
$f_{mf}, \tilde{f}_{mf}, \hat{f}_{mf}$	Micro forces
q_d , q	Position of micro object
$\dot{q}_d$, $\dot{q}$	Velocity of micro object
F_a	Applied force
r	Filtered tracking error
k_v, k	Gains of the PD controller
F_d	Disturbance forces
K_s	Spring constant of the cantilever
Δl	Cantilever deflection
$\ddot{q}_d$, $\ddot{q}$	Acceleration

e	Positioning error
$\dot{\boldsymbol{e}}$	Tracking of the positioning error
$W, \widetilde{W}, \widehat{W}, V, \tilde{V}, \hat{V}$	Neural network weight matrices
$\boldsymbol{\sigma}, \widehat{\boldsymbol{\sigma}}, \widetilde{\boldsymbol{\sigma}}$	Activation function at the hidden layer of neural networks
F_{cap}	Capillary forces
$\boldsymbol{F_w}$	van der Waals forces
F_{elc}	Electrostatic force
x	Neural network input vector
$q_B, \dot{q_B}, \ddot{q_B}$	Scalar bounds on position, velocity, and acceleration
X	Positioning command
c_1, c_2	Known scalar values
E_{RMS}	Root Mean Square (RMS) Error

Acronyms

Acronyms	Description
AFM	Atomic Force Microscopy
ANN	Artificial Neural Networks
BPL	Back Propagation Learning
DOF	Degree of Freedom
CMOS	Complementary Metal Oxide Semiconductor
DSP	Double-Sided Polishing
FOV	Field of View
GUI	Graphical User Interface
IC	Integrated Circuit
IPA	Isopropyl Alcohol
ITO	Indium Tim Oxide
MagLev	Magnetic Levitation
MEMS	Micro Electro Mechanical Systems
MLBP	Multilayer Back Propagation
MLP	Multilayer Perceptron
MOEMS	Micro Opto Electro Mechanical Systems
NEMS	Nano Electro Mechanical Systems
NN	Neural Networks
PID	Proportional-Integral-Derivative
RH	Relative Humidity
RMS	Root Mean Square
SISL	Stability in the Sense of Lyapunov
UUB	Uniform Ultimate Boundedness

Chapter 1

Introduction

This thesis is focused on high precision automated micro object manipulation and its applications in the serial positioning of micro size objects. The goal is realized by developing a nonlinear adaptive controller with a visual servo mechanism. The particular interest in designing such a controller lies in the need to compensate for surface micro forces. The micro objects, investigated in this thesis, have a flat surface of contact, and thus, are subject to relatively strong surface forces. A systematic investigation is proposed to characterize these micro forces. Then, a nonlinear adaptive controller is designed and its stability is proven. To verify the mathematical modelling, an automated micromanipulation of several micro objects is experimentally conducted.

In the literature, the term *micromanipulation* is used in the sense of the micro precision manipulation of objects including macro and milli size ones. In this thesis, *micromanipulation* is used exclusively for manipulating "micro size" objects. In the literature, the terms, *surface forces, micro forces, surface scaling forces* and *surface micro forces* are interchangeably used. However, in this thesis, the term "micro forces" is used to refer to these surface scaling forces.

1.1 Background

Micromanipulation is the positioning, moving, pushing, rotating, picking up and placing tiny components ranging from a micron to a millimetre. Since the Nobel Prize winner, R. Feynman, gave his famous speech in 1959, entitled "*There is Plenty of Room at the Bottom*", an increasing amount of research has been devoted to micromanipulation. In his talk, which was given only three months after the invention of the Integrated Circuit (IC) by Kilby from Texas Instruments, Feynman introduced the feasibility of "*manipulating and controlling things on a small scale*".

The primary motivation for developing Micro/Nano Electromechanical Systems (MEMS/NEMS) is the ever-increasing need to save energy and material that can be best achieved by developing almost weightless miniaturized devices. This has resulted in the advancement of surface machined-based microfabrication, which has made it possible to develop not only smaller microchips, but also various types of microsensors, microactuators, and lab-on-a-chip devices.

Although the development of microfabrication techniques resulted in substantial progress in the miniaturization of devices such as electronic circuits, these techniques are incapable of supporting 3-D structures. In general, research in MEMS still lags behind in terms of the development of reliable tools for post-fabrication processes by which the precise and dexterous manipulation of individual micro size objects is possible. Such a micromanipulation tool has applications in industry for the microassembly to create complex 3-D structures. Also, a reliable micromanipulation technology provides researchers with a tool for examining or altering micro objects, particularly biological samples.

The problem of automated micromanipulation is twofold. From the hardware perspective, manipulators, end effectors, actuators, sensors, and power supplies must be developed. Additionally, controllers must be designed and implemented if automated micromanipulation with a high precision is desired. Despite the efforts over the past decade in the area of micromanipulation, more research and development is vital in both the hardware and controller fields, until a reliable automated manipulation is realized.

The only automated micromanipulation which has been commercially available, is the microassembly of electronic chips. The manufacturing industry uses the well established automation techniques of macro robotics that readily controls and performs the path planning of the end effector. The high speed linear pneumatic actuators that have been widely used in the manufacturing industry for decades have come in handy in the rapid assembly of micro objects. Therefore, the hardware in such microassembly systems is the same as that used in the industry for several decades of automation in the conventional manufacturing of macro-parts. The only difference is that the end effector has been traded for a micro gripper to perform pick-and-place via a snap-and-lock mechanism. Since the actual task of micromanipulation does not introduce any significant forces to the actuators in macro-scale robots, no specific controller is required for the automation system to be applicable in the micro world. Consequently, there are no new challenges in the realization of micromanipulation in this type of microassembly.

However, the convenience of utilizing existing robotic technology in the micro world, where the governing forces are principally different, comes with some drawbacks.

- Micro objects cannot be arbitrarily positioned. Instead, they must be tethered to the substrate, and fixed to predefined locations.

- Special features must be added in designing these components to allow for the snap-lock mechanism during the process of manipulation. Applying such a mechanism is not always feasible, especially for soft tissues such as biological samples.
- The dimensions of grippers and micro components must satisfy very tight tolerances. Otherwise, the components can easily break if they are not perfectly aligned. This adds to the cost of the fabrication and setup.
- Current microassembly systems are expensive and have a relatively large footprint.
- Such systems do not provide enough dexterity, when it comes to fabricating more complex 3-D structures.

As a general rule in robotics, the following is pivotal in achieving a better dexterity in manipulating a component.

- The end effector must have several Degrees of Freedom (DOF) such as a wrist assembly.
- If the end effector has only one DOF, additional DOFs must be provided by other linkage(s) preceding the end effector. These links must have the same order of magnitude, in length, as the scale of the component under manipulation.

Although microgippers in microassembly have dimensions in micro scale, their actuation mechanisms often have one DOF. The additional DOFs in current microassembly systems are provided by other linear macro actuators. The long links in microassembly manipulators significantly limit the dexterity of the manipulation within a very small space, where the micro structure lies. Therefore, multi DOF microactuators and microrobots are the ideal hardware for dexterous micromanipulation.

Over the last decade, a number of micorobotics research labs have been established, and various microactuators and micro robots have been developed. These micro robots are either manually controlled, or their proper automation is limited to a specific system configuration. The literature does not comprise any research on the implementation of an effective controller for automated micromanipulation by using a microrobotic. The biggest challenge, regarding automated micromanipulation, has been the existence of micro forces that are dominant in micromanipulation, and barely known to researchers. Often, the arms and linkage in microactuators are compliant, and undergo a considerable amount of deflection during micromanipulation. Also, the power requirement of these microactuators is highly dependent on the micro forces exerted at the end effector. Therefore, the precise positioning of the end effectors during

micromanipulation is possible, only if a controller is implemented to effectively compensate for the micro forces in the process.

This thesis explores the problem of automated micromanipulation to accurately push and position micro objects by compliant micro structures. The chosen micro objects present a flat surface with a large contact area, and thus, large surface micro forces. After these forces are characterized, their complex nature and nonlinear behaviour are demonstrated. Then a novel adaptive nonlinear controller is designed and implemented to compensate for the surface micro forces during the micro object pushing operation. With such a controller, the fully automated sequential positioning of multiple micro objects on a flat substrate is performed. The results are analyzed for different control strategies.

1.2 Problem Statement

Despite advancements in MEMS over the last few decades, automated micromanipulation has not been realized. Available micromanipulation systems are prone to a variety of limitations. First, such technologies are expensive and come with a large footprint. Secondly, special design features must be added to the micro components to allow snap-lock mechanisms. Thirdly, these technologies are not capable of performing dexterous manipulation.

Other systems developed in research labs either require careful surveillance by an operator or are tele-operated [1]. Furthermore, for most existing systems, different trials must be carried out before the micro samples can be positioned accurately. This is a tedious and time consuming process for the micromanipulation tool.

To tackle these problems, we propose micromanipulators that are composed of microactuators instead of expensive high resolution macro-scale positioners. The primary challenge in the micromanipulation by using multi DOF microactuators is the controllability of the process, essential for the automation of a process with a high precision.

In micromanipulation, the gravitational force is surpassed by other dominant micro forces, such as van der Waals, capillary, electrostatic, and other adhesions. Despite some efforts to capture the mathematical model of these seemingly weak surface forces, much remains to be realized, before it would be possible to base a reliable micromanipulation controller on analytical or empirical models, representing the surface micro forces.

Therefore, the objective of this thesis is to realize an automated micro object manipulation, where the effect of the dominant micro forces is effectively compensated for in a nonlinear controller.

Microassembled devices can benefit from the proposed system including optical MEMS switches [2, 3], die level MEMS pressure sensors [4], and 3-D microelectrode arrays for applications in neural prostheses [5]. The proposed adaptive controller eliminates the need for an operator's surveillance, resulting in increased productivity. Moreover, the proposed manipulation strategy exhibits less variability than human operators, resulting in a greater control and consistency of the product quality of 3-D MEMS devices.

1.3 Thesis Objectives

This research comprises several tasks.

- Design an inexpensive experimental setup as a platform for the force characterization that is highly appropriate for micro scale objects, and replaces Atomic Force Microscopy.
- Characterize the surface scaling forces between the surface of square-shaped silicon micro cubes, silicon and a glass substrate during pushing, and demonstrate the complexity of their behaviour, when the ambient condition changes.
- Develop an adaptive nonlinear controller that is capable of pushing and precisely positioning micro objects with an arbitrary size and under varying operational conditions.
- Compare the accuracy of the proposed controller with conventional linear controllers by conducting experiments.
- Realize the fully automated controlled positioning of micro objects with different sizes and surface conditions in varying operational ambient conditions as a part of a microassembly line.

1.4 Contribution

The thesis proposes a neural network (NN)-based adaptive controller for the automated positioning of micro size objects by using compliant micromanipulators. Unlike available micromanipulation systems, no human intervention is required, and the adaptive controller is robust under varying operational condition. Micro objects can be of any size and shape with any surface characteristics, and the proposed

controller provides compensation for the micro forces and push micro objects with precision along a desired trajectory. We also propose an experimental setup that relies on visual feedback and a slim cantilever to quantitatively and reliably measure the forces in the micro scale. With the experimental setup, the surface forces, resulting from van der Waals and capillary forces in the micro domain are characterized under varying ambient conditions.

The proposed experimental setup does not require tedious calibration procedures that AFM users encounter, and as such, is an attractive alternative for MEMS researchers. Previous micro forces characterization studies have been conducted in a highly controlled environment on nano –size spherical particles by using AFM. The objects considered in this thesis are square-shaped, and therefore, present a larger contact area than those of their spherical counterparts. This strategy ensures that the impact of the scaling forces is more significant. Although the controller design is more challenging, it is practical and applicable. The specific contributions of the thesis are as summarized as following.

- An inexpensive easy-to-use experimental setup is proposed for the reliable quantitative characterization of the collective surface forces, involved in pushing micro size object
- Micro forces in the interface between the flat micro objects with various sizes, and substrates with different materials under varying ambient conditions are qualitatively characterized.
- An adaptive nonlinear NN-based controller is designed to compensate for the micro forces during manipulation.
- The performance of the proposed controller is verified experimentally by pushing micro objects.
- The fully automated precise sequential pushing of micro objects along a desired path is realized.

1.5 Thesis Organization

The first task is to analyze the surface scaling forces which are present at the interface between the micro objects and substrate. Experiments are conducted to characterize the aggregated micro forces, including capillary and van der Waals forces. These forces collectively form an interfacial shear strength between the flat micro components and a flat substrate during the process of micro scale object pushing. The relationship between the magnitude of the surface forces, and the parameters, including the velocity of the

pushing, relative humidity, temperature, hydrophilicity of the substrate, and surface area, is also empirically investigated. Also, an inexpensive experimental setup is built, as a platform to replace Atomic Force Microscopy for force characterization of micro scale parts.

In the second part of this thesis, an adaptive NN is proposed for micro object manipulation. This thesis presents the first experimental application of automated micro pushing.

This thesis continues with the following chapters. Chapter 2 provides a comprehensive review of the micromanipulation in the literature and introduces the necessary background of both the physics and mathematics of the micromanipulation problem, and more precisely, different models of micro forces are reviewed. In addition, artificial NN and their applications in modelling micro forces, are presented. In Chapter 3, the experimental setup is described, system calibration and sample preparation procedure are elaborated on, and micro forces characterization under varying operational conditions is obtained. Chapter 4 provides details on the design of the new adaptive NN-based controller, and its stability is mathematically proven. In Chapter 5, the developed control system is implemented in the sequential micromanipulation of three micro objects to position them accurately and autonomously on a substrate. In addition, the performance of the proposed controller is compared with that of conventional open-loop and linear closed loop controllers. Finally, Chapter 6 provides a discussion of the results, applications, and plans for future work, and concludes the thesis.

Chapter 2

Background

2.1 Introduction

In this chapter, previous research in the area of micromanipulation is reviewed. Then a summary of surface micro forces that are present in the micromanipulation is provided. Also, their mathematical models in the literature are discussed. The last part of this chapter introduces NN and their universal function approximation properties.

2.2 Literature Review

2.2.1 Applications of Micromanipulation

In recent years, research efforts in the development of MEMS and micro object manipulators have increased dramatically. Nanomanipulation has been utilized in such applications as plasmonic device prototyping [6], building templates such as stamps or molds and manufacturing micro pattern [7], prototyping single electron transistors [8], and manipulating biological cells and molecules [9, 10]. By precisely controlling nanomaterials including quantum dots and biomolecules, Tafazzoli formed micro patterns of a defined shape and distribution via a force-controlled micro stamping. This work has applications in molecular circuits, as well as cell spreading and adhesion studies [7].

Microassembly, as one of the most appealing applications of micromanipulation, can substantially expand the micromanipulaton application area. Micro optics in communication is a common example of applications which can benefit from this approach. In some recent works, micromanipulation was utilized in developing optical switches and Micro-Opto-Electomechanical Systems (MOEMS) [11, 12]. Microassembly is inevitable in the development of MOEMS because of the incompatibility of optics devices with CMOS technology.

Other significant applications of autonomous microassembled systems can be seen in biomedicine such as microsurgery[13-15], cell manipulation [16, 17], cell healing [13, 18], and drug delivery [19].

2.2.2 Micromanipulation Techniques

Micromanipulation can take one of the following forms: pick-and- place (release), rearrange (rotate, turn, ..), and push-and-pull.

The complexity of the surface forces and the lack of an analytical model to predict the dynamics of micro objects under manipulation have led most researchers to adopt specific manipulation techniques instead of generic ones to accomplish micromanipulation. Non-contact manipulation has been carried out by the magnetic levitation (MagLev) of objects [20-22]. Although MagLev can eliminate the complex problem of micro surface forces through manipulation, MagLev cannot completely eliminate the objects in contact with another material at the start and target point of micro object positioning. Maglev also requires equipment with a large foot print and high power. More importantly, magnetic force is a body force which is almost negligible when the size of the objects is less than a millimetre.

Sinan et al have exploited the expansion and contraction of air trapped in a micro hole for picking and releasing micro objects. They took advantage of the scaling laws by miniaturizing the end effecter to favourably reduce the time constant of the heat transfer [23]. A similar idea has been used by other researchers who utilized pressure change, caused by the temperature change inside the micro holes on the end effecter surface [24].

The use of adhesions to control micro parts has also been reported [25]. Electrostatic force was utilized to detach the particles from the substrate and Van der Waals force was used to attach the particle to the substrate, or vice versa. However, by using this method, a successful manipulation requires an ad-hoc process to adjust the critical distance of the AFM tip and the particle, because there is no accurate modelling for comparing van der Waals with electrostatic forces. The size of the objects, which have been reliably picked up and released by controlling the adhesion, has been no less than hundreds of micrometres [26]. Also, manipulation methods based on the potential gradients (capillary, electric field) have been used [27]. It was demonstrated that the proposed manipulation technique was applicable only for objects larger than 300μm [27]. For these specific techniques that rely on self-alignment and self-assembly, a very special preparation and laborious requirements must be met. However, this substantially limits the practicability of the technique. Moreover, as the micro object size becomes smaller, the

complexity of the micro forces and handling them increase considerably, making it unreliable to use adhesions for controlled micromanipulation.

Micromanipulation in aqueous environment has been studied. Chan et al made a trimorph thermal actuator to grasp the biological cells in liquid environment [28]. They used a type of polymer which is bio-compatible. *Danio rerio follicles* in a fluidic medium have been captured successfully by using their proposed actuators. Aligning micro particle in a liquid media was carried out by using acoustic force (ultrasound field). A micro gripper can then enter the fluid and pick up particles automatically at a fixed location. The objects were sphere suspended in de-ionized water [29]. Adhesion-based cell manipulation, including the capture and separation of cells in microfluidic devices has been reported [30]. In this work, the manipulation is mediated by a special class of adhesion proteins on the cell membranes. It is common for biologists to use a pipette and agarose gel for cell isolation, manipulation and micro injection. However, it is more convenient to grasp a cell and carry out the injection by using a microgripper.

Soon after its development, AFM has attracted researchers in micro robotic labs to perform the controlled pushing operation [25, 31]. It should be mentioned that, although AFM has proven successful in micro and nanomanipulation, it is technically over designed for micromanipulation. The commercial versions of AFM are too sensitive and require stiffer cantilevers for micromanipulation. Most of the researchers have either added more features (optical and camera) to the chamber, or have made a custom-designed AFM, leading to even more expense. A tedious procedure is also required to calibrate the machine and obtain a meaningful voltage-distance curve [32]. Moreover, AFM is only useful for pushing, and can be hardly used for pick-and-placing. Consequently, AFM machines are not appropriate for mass microassembly robotics.

The most generic and straight forward method for micromanipulation is based on designing appropriate microgrippers for picking and placing, and a sharp tip for pushing. For autonomous pick-and-place purposes, Thompson and Fearing have used two orthogonal piezoelectric tips, each equipped with a strain gauge to provide contact force feedback. This tip is capable of manipulating blocks as small as 200 μm. The authors have developed a step-by-step manipulation algorithm by studying the behaviour of the block under manipulation with two perpendicular tips [26]. A similar idea has been applied to rotate gripped micro objects [33].

The use of vibration is one of the most promising and practical methods to reduce stiction [34] and release objects [35]. The ultrasonically-aided release of micro objects, stuck to a gripper finger, has also been demonstrated [29].

2.2.3 Micromanipulation Precision Control

The extremely low inertia of microactuators has granted them high resonant frequencies which are potentially desirable for the high speed actuation, required in MOEMS and other applications. The scaling law has elevated the influence of surface forces in bearings, gripper-component and component-substrate surfaces significantly. A very limited understanding of those effects has been achieved. Although MEMS studies have been mostly directed to novel designs and actuation mechanisms to improve the yield rate, actuation stroke, power consumption, miniaturization, and packaging, some researchers have targeted the high precision control of MEMS devices. Shih-Chi Chen has showed an enhanced dynamic performance of a micro scale, six-axis nanopositioner via *Input Shaping*. Input Shaping is the trade-name for a robust feedforward technique for preventing motion-driven vibrations in high speed systems. Using this method resolves the problem of overshooting which is caused by the intrinsic characteristic of low-damped silicon-based micro structures [36].

The precise micro-macro pushing of some ferromagnetic micro objects has been demonstrated by moving and rotating a magnet, located under the substrate. The controller consists of three specialized PI controllers for each of the following manipulation steps: approach, coarse positioning, and fine positioning [37].

For trajectory control, or more precisely, for target position control, a computer vision-based method can be used [17]. The position of the object was acquired via a CCD camera.

The most common way of precisely manipulating micro objects has been ad-hoc methods which incorporate a micro/nano force sensors at the tip of microgrippers [26, 31, 38-40]. This provides the controller with the useful information of the relative position of the micro object with respect to the tip of the manipulator/gripper. Based on this feedback, the central processor knows if the object is either out of contact, just in contact, or being gripped with the tip. Then the processor can apply the appropriate control algorithm [31] to adjust the applied force by the actuator to prevent the micro object from possible damage [38]. Although incorporating tactile sensors into micromanipulators seems to be essential for an

autonomous stand-alone microrobotic system, it is not sufficient if a controlled trajectory of the manipulated micro components is desired. Furthermore, depending on the size of the objects and ambient conditions, the forces generated from a micro tip pushing against a micro object can be in the scale of nano or even piconewton. Detecting the magnitude of the forces in the presence of noise remains a challenge for engineers. Some efforts devoted to micro force sensing are reviewed in the following section.

2.2.4 Micro Forces Characterization by MEMS

The integration of touch sensor on the gripping area of microactuators has been the subject of recent research in the enhancement of micro and milli robotic systems. A highly sensitive axis force and force rate sensor by using polyvinylidene fluoride (PVDF) has been developed [41]. It can provide reliable measurements of the contact forces at the sub micronewton scale. Thompson and Fearing embedded a strain gauge at the tip to detect forces as small as 0.4 millinewton [26]. In principle, the slender cantilevers are the basis of measuring forces. Consequently, AFM is the best candidate, if accurate molecular scale force measurement and tribological characterization is concerned [32, 42]. Since commercial AFM has not been designed for lateral pushing, most labs have built customized systems, especially when the objects are larger than a few micrometre [43]. Other cantilever-based micro force sensors have also been prototyped [44]. By replacing longitudinal cantilevers with micromachined torsional oscillators, Lopez et al have increased the sensitivity of MEMS-based force sensors to piconewton [45]. An inverse comb-drive actuator has been employed as a stand-alone micro force sensor to measure forces as low as a micronewton [39, 46]. Jeong et al have replaced laser optics with a high-magnification vision system to measure the deflection of a slender cantilever [47]. All these force sensors demand an accurate calibration, if surface force characterization is to be carried out for a quantitative assessment.

2.2.5 Autonomous Micromanipulation

MEMS technology has enabled scientists and engineers to mechanically manipulate objects as small as a few hundred of nanometres by using micro grippers and tweezers with a very fine tip. High precision robotics and stages, driven by stepper-motors with advanced microstepping technology, have allowed for the motion of miniaturized tips with submicrometre step size (typically 0.04μm by *Sutter*). These advancements have made it possible to build a semi-autonomous tele-operated micromanipulation

workstation [1, 48]. The intervention of a human is necessary to correct the actions by observing the instant states of micro particles which are quite unpredictable.

Researchers have focused on automating the micromanipulation process by developing novel micro force sensing and control techniques [38].The only fully automated nano particle manipulation in the literature has been demonstrated by using AFM [31, 43, 49]. AFM has the unique feature of providing both contact force and topography of the manipulation site. This feature makes AFM the device of choice for autonomous nanoparticle manipulation. Besides haptics, the topography data is critical if position control is desired. However, AFM manipulation is time-consuming, expensive and the calibration is labour intensive. Moreover, AFM has not been used for micro size object manipulation due to its high sensitivity to pico scale forces. Recent advancement in machine vision means the operator is replaced by a CCD camera and image processing algorithms, embedded in the microcontrollers [17]. The authors have developed an autonomous embryo pronuclei DNA injection micro robotic by using visual servoing and precise motion control. The controller, despite its high yield, does not compensate for micro forces because the cell is already fixed and the DNA is carried in a pipette. Their recent work on visual servoing addresses nanopositioning of the tip of a microactuator, which is operated under zero load (no micro object manipulation) [50].

2.2.6 Multi Degree-of-Freedom Microactuators

Similar to macro robotics, multiple DOF of motion are necessary to enhance the dexterity of the micromanipulators. Conventional surface micromachining processes, in essence, fabricate planar structures which are mostly confined to 1-D motion. Although out-of-plane actuation has been achieved in several labs [51-53], it remains uni-dimensional. Some notable examples of multi DOF micro mechanisms have been reported [54, 55]. In the first work, a small-scale nanopositioner, called μHexFlex is designed and fabricated. This mechanism has six DOF; three translational and three rotary. The entire system comprises a six-axis compliant mechanism and three pairs of two-axis thermo-mechanical microactuators, all fabricated by CMOS surface machining technology. However, μHexFlex is only a precise MEMS positioner, incapable of manipulating random micro objects. Similarly, the idea of linking multiple planar piston-like translational movement by means of flexure beams has been used to create out-of-plane motion [55]. The MEMS out-of-plane mechanism, which is designed for optical application,

acts as a stage, not a micromanipulator. Some techniques has been used to realize a mobile miniaturized actuator [56]. It is an electrostatic-driven milli size walking robot. The notable part in this work is the 8.5mm two-legged inchworm robot with a power-supply (solar cell) and controller on board. Nevertheless, the practical motion of this insect-like robot has been shown to be poor. The on-board power supply for each axis is a good approach for constructing a microassembled multi-DOF manipulator, since powering all the axes via one base arm is challenging.

2.2.7 Microassembly Systems

During the last decade, special interest has been devoted to microassembly and its applications. Various approaches and their advantages and disadvantages have been presented in a conference by a group of researchers from academia and the MEMS industry [57]. Serial assembly, parallel assembly, self-assembly, wafer-to-wafer transfer, stochastic microassembly, and packaging are among the concepts briefly discussed. With current technology, all the microassembly methods have been carried out by tele-manipulation, that is, the process is entirely monitored by an operator who can intervene at any time. Perhaps the most notable microassembly robotic station has been developed by Dechev and his colleagues [1]. They first integrated a passive microgripper in the tip of a multi-DOF robotic positioner. It can pick up and assemble other micro parts which were "Designed for Assembly (DFA)" to fit into a snap-and-lock mechanism. The authors' more recent work has focused on developing the gripper as an active actuator to allow the realization of a more generic microassembly system to pick up a wide range of micro objects. This method has been adopted to microassemble complicated 3-D structures [11]. These methods are all based on tele-manipulation.

Using two orthogonal tips, equipped with a force sensor, and following recent grasping and rotating algorithms, an assembly of sub-milli size blocks in the desired orientation has been successfully illustrated [26]. Heating elements are used on the surface to melt and cool the wax for bonding the micro parts. Figure 2-1 displays one of the 3-D structures that is autonomously assembled [26]. The dimensions are in the order of 200μm.

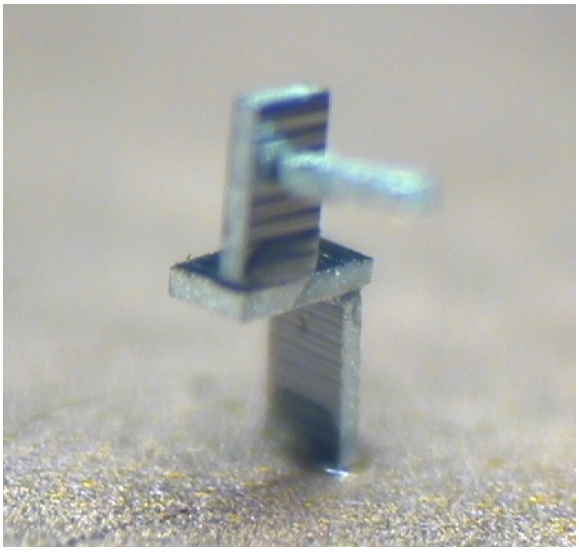

Figure 2-1: Stacked microassembled micro parts, bonded with UV cure epoxy. Three large base parts are 400µm x 230µm x 75µm, and the top part is 80µm x 80µm x 430µm [26].

Self-assembly in an aqueous environment has been investigated. At the molecular level, some techniques are applicable for molecular electronic and bioelectronics devices, where the materials are aligned by electric field, Langmuir-Blodgett techniques, or mixing with liquid crystals [58]. Most of these methods exhibits a restriction in their patterns and molecular orientations [58]. Other fluidic self-assembly techniques are also developed [59, 60]. As for self-assembly in a sub-millimetre range, capillary forces are used to self-align close-to-a-millimetre size blocks on top of each other. The parts follow the equilibrium capillary force and are positioned at an equal distance from the edges of the block underneath [61].

Some creative methods have been published which avoid assembly by deforming planar flexible structures to create out-of-plane 3-D devices. Deformation can be performed either by a mechanical contact tool [62], or non-contact methods such as centrifugal forces [63].

Parallel assembly, in which large ensembles of micro parts can be assembled simultaneously, was implemented [57, 64]. The authors designed and fabricated an assembly station that presses pins with a diameter of 386µm and 485µm into a LIGA substrate and then adds a 3-inch diameter wafer with LIGA gears on the pins [64].

Funded by the European Commission and started in 1998, a collaborative multi-stage program of research from seven European countries to develop intelligent micromanipulation and micro robotics. In the first phase, a "MiniMan" was made. MiniMan was a piezo-actuated decimetre size mobile robot, providing a platform for the assembly of milli size parts [65]. A vision algorithm for the micromanipulation, related to this project, is published [66]. Titled MiCRoN, the second project was introduced to develop a cluster (5 to 10) of small (scale of cm^3) mobile autonomous robots. These wireless agents, each equipped with onboard electronics, co-operate in a desktop environment to execute a range of tasks associated with assembly and processing from the nano to the micro range. To the best of our knowledge, these projects have not been successfully realized, yet. The most recent project of this chain is called I-Swarm. This name reflects the objective of a microrobot swarm for the execution of a collective task by a thousand micro manufactured autonomous robots. Some publications do reflect the polymer-based type of actuator relevant to this milli size robot [67]. Also, an investigation of the feasibility of inductive communication among the 1mm x 1mm x 2mm mobile robots have been presented [68].

2.3 Surface Micro Forces

Considerable effort has been reported in the literature to formulate micro forces. Most of the proposed formulas consider the same set of variables for a specific type of micro forces. Yet they vary in representation [69, 70]. Furthermore, these forces have been dealt with individually and the interaction among them remains unknown. In this thesis, the term *micro forces,* is allocated to any force which opposes the movement of the micro object, which is being pushed on a substrate. Micro forces exhibit static, viscous, stick-slip and stribeck behaviour [71], and include adhesive forces such as capillary, van der Waals, electrostatic force, or any combination of them. In what follows, a brief description of the most common micro forces is provided.

2.3.1 Conventional Friction

The models reported in the literature for conventional friction consist of a number of coefficients that corresponds to various parameters such as viscous, Coulomb and static friction, the stribeck effect, and the stick-slip behaviour of friction [71, 72]. Those models are difficult to implement, because the aforementioned coefficients are difficult to measure. However, the dependency of the friction on the applied force (for the static state) and velocity is obvious [71, 72]. Friction has been also found to be highly altered by ambient conditions [27, 73, 74]. A preliminary study of the friction measurement in MEMS has revealed that the coefficient of friction in air is much higher than that in a vacuum. Depending on the materials in contact, this trend varies. For instance, hydrophilic materials tend to adsorb more moisture than hydrophobic ones, resulting in a greater capillary force. In addition, native oxide on the surface plays an important role in increasing friction coefficient [75]. Other experiments suggest that surface contamination, due to the air composition, is another source of friction [75].

Some tribologists have looked at the friction from another perspective. Through some well-known mechanisms, friction has been attributed to plowing the asperities of the harder material through the softer one, and shearing the junction, formed at the region of contact [70, 76]. With some reasonable simplifications, this shearing friction force is defined as a function of Young's modulus and the Poisson ratio of the materials of the two surfaces, the pressing force, the number of contact points, and the surface roughness [77].

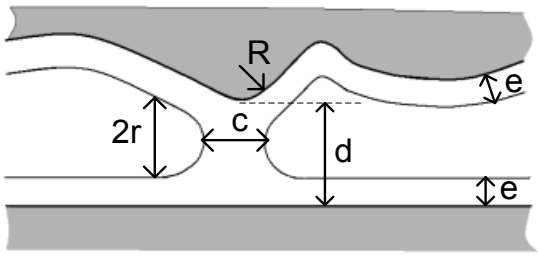

Figure 2-2. Liquid bridge formed between a rough surface and a flat surface. A layer of moisture with the thickness of *e* covers the two surfaces.

2.3.2 Capillary Forces

From a microscopic point of view, a thin water layer exists on the surface of most materials exposed to air. Due to the surface tension property, a liquid bridge is created between the two surfaces, approaching

or retracting from each other, as shown in Figure 2-2, and in turn, produces an adhesive force. Provided that r ≪ c ≪ R in Figure 2-2, this force can be estimated by computing [78]:

$$F_{cap}(d) = 4\pi\gamma R(1 - \frac{d - 2e}{2r}) \quad . \quad (2.1)$$

The parameters of this capillary force are the surface-tip distance *d*, radius of the curvature of the meniscus *r*, radius of the tip, *R*, the thickness of the liquid layer, *e,* and liquid surface energy, γ , (for water $\gamma = 72\text{mJ/m}^2$) [78]. The topographical features are correlated with the surface roughness parameter of R_a and contact area, *A*. By definition, R_a is the arithmetic average of the surface profile amplitude. The thickness of the liquid layer is also proportional to the relative humidity, *RH*, of the atmosphere. Thus, the capillary force between two surfaces of the given materials is a function of the surface roughness, contact area, and relative humidity. In other words:

$$F_{cap} = f(R_a, RH, A) \quad . \quad (2.2)$$

2.3.3 Van der Waals Force

One of the dominant interactive forces in the micro domain is the van der Waals. This force becomes more dominant as the size of the part drops below 10 micrometres. Van der Waals force occurs by a momentary dipole moment between the atoms, resulting from the interaction among the electrons rotating in the outermost bands. In spite of all efforts to clarify the associated equation, van der Waals force has remained relatively unknown due to its interaction with other micro forces. By ignoring the effect of the capillary force, a typical expression of this force between the asperity and the flat surface, depicted in Figure 2-2, is as follows [79]:

$$F_w = \frac{2HR^3}{3d^2(d + 2R)^2} \quad , \quad (2.3)$$

where *H* is the *Hamaker* constant. The power of the distance, *d,* significantly depends on the order of the proximity. For distances greater than 50 nanometres, van der Waals force is inversely proportional to d^6 due to the retarded van der Waals effect [80]. Therefore, (2.3) is not a unique expression proposed in the literature for van der Waals force. For a flat micro object, resting on a substrate, there is a correlation between van der Waals force and the surface roughness.

2.3.4 Electrostatic Force

Compared to other micro forces, electrostatic force is well understood in the literature, and is a function of the electrical charges, q_1 and q_2 , of two surfaces separated by distance d such that

$$F_{elc} = \frac{q_1 \cdot q_2}{4\pi\varepsilon_0 d^2}, \qquad (2.4)$$

where ε_0 is the permittivity of the free space. By grounding the surfaces, this force can be eliminated.

2.4 Artificial Neural Networks Models for Function Approximation

Artificial NN architecture with their numerical learning capability has been the subject of countless investigations in the past few decades. The effectiveness of NN as a black-box in compensation for the unknown, nonlinear friction force in conventional robot trajectory tracking problems, has been presented in the literature [81]. Usually, the friction in macro systems counts for only a small proportion of the system dynamics. Friction is often treated as a disturbance or noise in the controller loop. In contrast, micromanipulation deals with a system whose response almost entirely stems from the non-inertia forces. As such, the application of artificial NN to represent those forces is a novel approach which requires systematic designing.

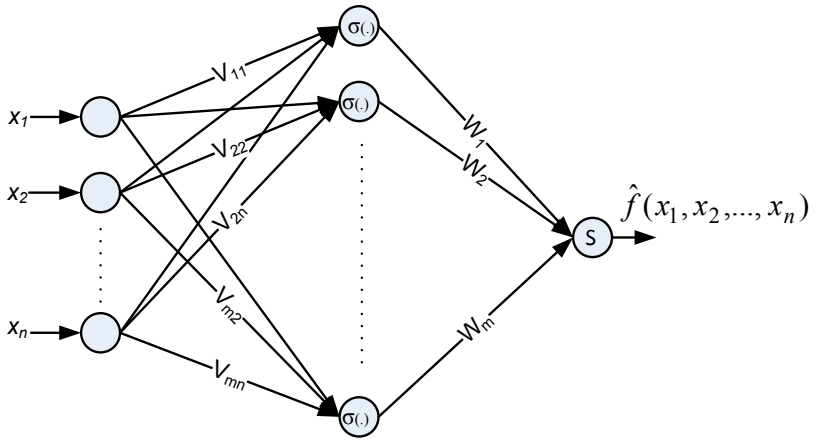

Figure 2-3. Two layer neural network with linear activation function at the output node.

Figure 2-3 denotes a two layer feedforward NN with a linear activation function in the output layer. The output, $\hat{f}$, is an approximation of the function, $f = (x_1, x_2, ..., x_n)$. Learning occurs when the free

parameters of the network, that is, the connecting weight matrices V and W, are adapted through a continuous process of stimulation by the environment in which the network is embedded. The free parameters are the network weights which represent the weighted strength of each synaptic or connection between two neurons in the neighbouring layers. The weight between neuron i in layer $L+1$ and neuron j in layer L can be updated as

$$W_{ij}(k+1) = W_{ij}(k) + \delta W_{ij}(k) \quad , \quad (2.5)$$

where k is the time index (the iteration number) and δW_{ij} is the weight change at the time step, k.

Different environments, that is, different applications of the NN, impose different adaptation algorithms. A comprehensive investigation of such methods has been presented [82]. In a multilayer perceptron NN, a gradient descent technique, called backpropagation learning (BPL), is chosen to minimize the cumulative errors of the NN output values compared to the desired values [82]. A multilayer NN with this learning algorithm is called a Multilayer Back Propagation Neural Networks (MLBP).

2.4.1 Universal Approximation of MLBP Neural Networks

In this thesis, the particular interest in the multilayer NN lies in its key property of Universal Function Approximation (UFA) [83, 84]. Any continuous nonlinear function can be approximated by such intensive networks, distributed and operating in parallel. The Stone-Weierstrass theorem proves that the multilayer perceptron (MLP) NN are capable of uniformly approximating any real continuous function on a compact set to an arbitrary degree of accuracy. This theorem states that for any given real continuous function f on a compact set $U \subset R^n$ there exists a network F that is an approximate realization of the function $f(.)$ expressed as

$$F(x_1, \dots, x_n) = \sum_{i=1}^{m} \omega_i \varphi\left(\sum_{J=1}^{n} v_{ij} x_j - \theta_i\right),$$

where

$$\left|F(x_1, \dots, x_p) - f(x_1, \dots, x_p)\right| < \varepsilon,$$

and $X = (x_1, \dots, x_p) \in U$ represents the input space, and ε denotes the approximation error for all $(x_1, \dots, x_p)$ in U which is a very small positive value.

Chapter 3

Characterization of Surface Micro Forces

3.1 Introduction

The purpose of this chapter is to provide a detailed procedure for reliably measuring complex surface micro forces during the process of pushing flat micro size objects on a flat substrate. In order to characterize micro forces under varying operational conditions, parameters such as relative humidity, temperature, velocity of motion, size of the contact area, and substrate material are altered to explore their effects on the surface forces. This chapter also introduces an easy-to-calibrate experimental setup which can be adopted by other researchers as a platform to accurately quantify surface forces during the manipulation of micro objects. The developers of micromanipulation systems for applications, including microassembly and manipulation of biological samples, can benefit from the findings of this thesis to control and automate the process of precise micromanipulation.

3.2 Scale Speed

Scale speed has been used in Radio-Controlled vehicles and toy models to measure how fast the RC vehicle travels in relation to the full size model. This definition is slightly modified in this thesis. Let's define the scale speed v_{ss} to be the real speed V_{actual} of a moving object, divided by its dimension *d* in the direction of the movement as

$$v_{ss} = \frac{V_{actual}}{d} \quad . \quad (3.1)$$

The scale speed has the dimension of sec^{-1}, commonly known as *Hertz* or *Hz*. Therefore, the scale speed can be thought of as the frequency at which a moving system travels the distance of its own length. This definition has a direct implication for estimating the productivity of manipulators in different applications such as the serial assembly of components. In assembly workstations, mechanical manipulators are required to travel further than their own length -and the part's length - in order to reach

different parts and assemble them sequentially. The productivity of such assembly factory does not depend only on the actual speed of the manipulators, but also on the size of the components of the system. Table 3-3 lists the scale speeds of various moving objects with different dimensional scales. The linear actuator offered by *FESTO*, for example, provides a relatively high productivity owing to its high scale speed of 100 *Hz*. On the other hand, a tortoise with the low scale speed of 0.36*Hz* is not as productive in building its own home. In this thesis, the scale speed of manipulation in the micro scale is determined for the pushing process and compared with the other data in Table 3-3.

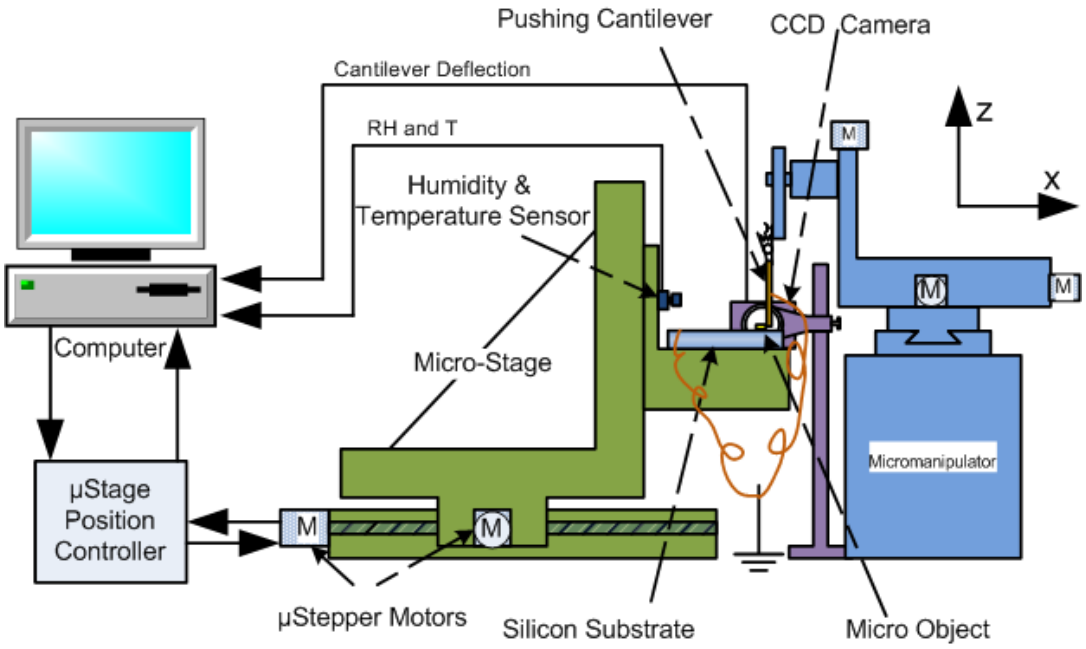

Figure 3-1. Block diagram of the experimental setup for micro forces characterization.

3.3 Experimental Setup

3.3.1 Hardware Setup

Figure 3-1 reflects the experimental setup, developed to characterize the surface micro forces, dominant in micro object pushing on a substrate. The hardware specifications are listed in Table 3-1. A silicon micro object is sitting on a substrate which is in turn placed on a micro-stepper-motor-driven stage. Two substrates are used: a DSP silicon wafer and Indium Tin Oxide (ITO)-coated glass. A silicon cantilever

tip is fixed from one end and pushes the micro object from its other end. To push the micro object, the stage is allowed to move the micro object against the micro tip, achieving the necessary contact and displacing the micro object along the x axis.

A high-definition CCD camera, mounted on a high magnifying zoom lens, is installed next to the stage, and aligned along the y axis. The camera is connected to a personal computer via a video acquisition board, where programs with the Graphical User Interface (GUI) are run. Attached to the microstage is a humidity-temperature sensor which monitors the ambient conditions in real time. The ambient conditions data are then collected via the GUI.

Table 3-1. List of hardware specifications.

Hardware	**Specifications**
Micro stage	Translational resolution: 0.156μm Velocity resolution: 0.745μm/sec
Vision system (CCD Camera + lens)	Resolution: 0.85μm/pixel Field of view: 640 x 480 pxls=545 x 415μm
Temperature sensor Relative humidity (RH) sensor	Resolution: 0.1 Celsius Resolution: 0.1%
Micro objects (4 sizes)	L100 × W100 × Thk50 μm L120 × W120 × Thk50 μm L150 × W150 × Thk50 μm L200 × W200 × Thk50 μm All diced out of DSP Si Wafer
Micro cantilever (3 sizes)	L16300 × W200 × Thk50 μm, Stiffness=0.2177 μN/μm L28700 × W200 × Thk50 μm, Stiffness=0.0396 μN/μm L38250 × W200 × Thk50 μm, Stiffness=0.0167 μN/μm All diced out of 50 μm Thick DSP Si Wafer
Substrate (two materials)	Silicon wafer ITO-coated glass

To minimize the effect of the electrostatic charges during the pushing, the substrate and the cantilever are wired to a common ground. The whole system is covered by an enclosure and placed on a vibration-isolated optical table. This experimental setup is depicted in Figure 3-2. The chamber is closed during the pushing experiment to help stabilize the ambient conditions inside. The hardware configuration, including the micro stage, micromanipulator, camera, and temperature-humidity sensor is placed on the grounded optical table. The 200μm-wide slim cantilever is vertically supported from its upper end by the clip, clamped on the micromanipulator. The micro cube lies on the glass substrate which is supported by the position-controlled micro stage. The horizontal applied force vector undergoes an approximate 8º change of angle due to the cantilever's deflection. To account for this deflection during pushing, the cantilever is

inclined, according to Figure 3-2(d) by 4º. This inclination is intended to retain the effective pushing force horizontal throughout the experiment.

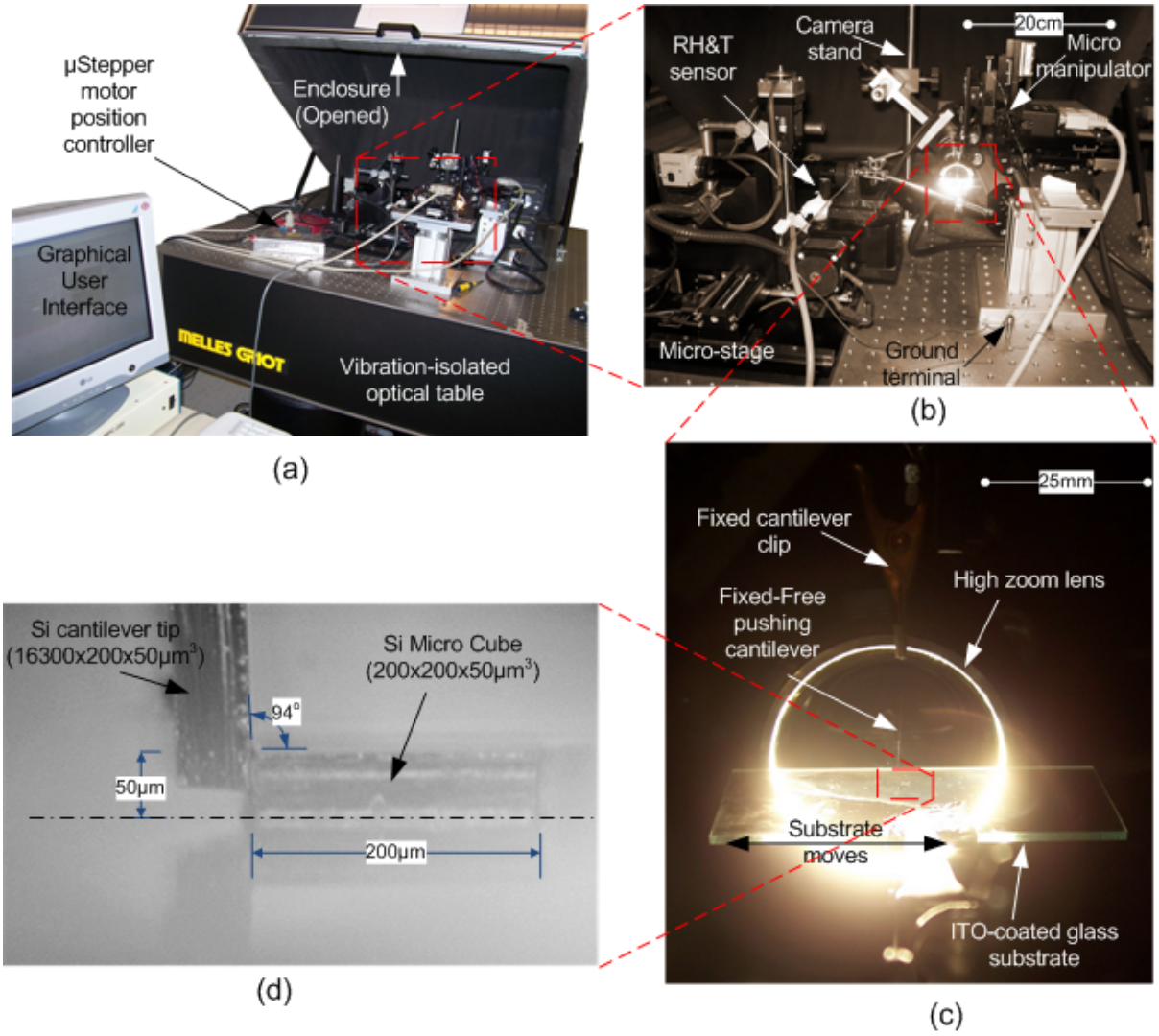

Figure 3-2. Experimental setup: (a) the hardware setup, (b) configuration of the hardware components, (c) the slim cantilever, vertically supported from its upper end by the clip, and (d) the high-zoom frame at the start of the pushing process. The blurry reflection of the micro cube and cantilever tip are seen in the substrate.

To facilitate the positioning of the micro cubes on the substrate and detach it from the cantilever, a needle with a sharp tip is employed (Figure 3-3). The minimal interface between the flat micro cube and

the sharp needle compared to the large interface between the micro cube and the substrate, significantly favours releasing the micro cube from the tip. The sharp tip is mounted on a secondary micromanipulation system (not depicted in Figure 3-1 and Figure 3-2).

3.3.2 Controller Design

Figure 3-4 illustrates the controller approach to push the micro object and log the data about the process. The user can set any arbitrary trajectory for the stage to move the micro object against the micro cantilever. The fixed cantilever then makes the necessary contact and pushes the micro object in the opposite direction. The real position and velocity of the micro cube, in pushing, is measured visually in this experiment. The frames grabbed from the CCD camera are fed into an image processing program to detect the edges of the micro cube and the cantilever. We adopt the canny edge detection algorithm, available from open source OpenCV libraries, for this application. The parameters of the canny algorithm, designed for this experiment, are listed in Table 3-2.

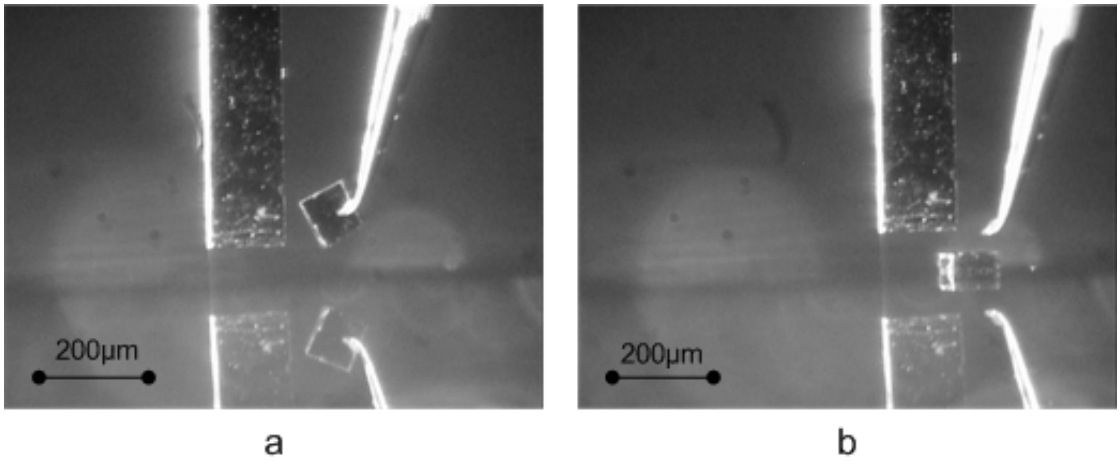

Figure 3-3. Placement and alignment of the micro cubes on the substrate: (a) a 120µm x 120µm x 50µm micro cube is picked up by the needle and (b) the micro cube is easily released from the sharp tip after attaining a larger contact with the substrate than the needle tip.

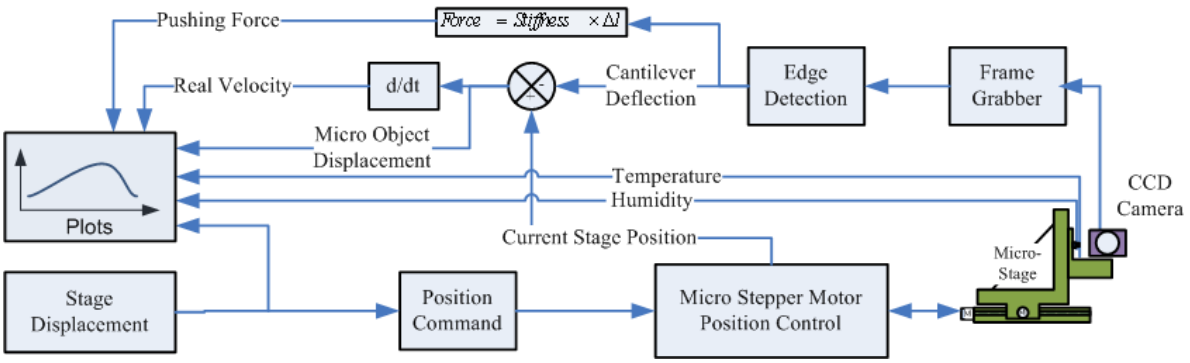

Figure 3-4. Experimental setup controller for micro forces characterization.

Figure 3-5 depicts a frame grabbed during the pushing and its canny-image-processed edges. As seen in this figure, the pixel of interest, along the detected edges, is also marked by the software. As a result, the deflection of the cantilever can be calculated, based on this pixel location. Consequently, given the exact position of the micro-stepper motor-driven stage at any time instant, the real displacement of the micro cube is calculated in real time by using this method.

Table 3-2. List of software specifications for micro forces characterization.

Real time data acquisition frequency	2Hz
Edge detection algorithm	cvCanny High threshold:15000 Low threshold: 5000 Sobel kernel size: 7
Maximum measurement error of real position (edge detection error)	±2pxl = ±1.70 µm
Microstage velocity threshold	$v \leq 7.5$ µm/sec

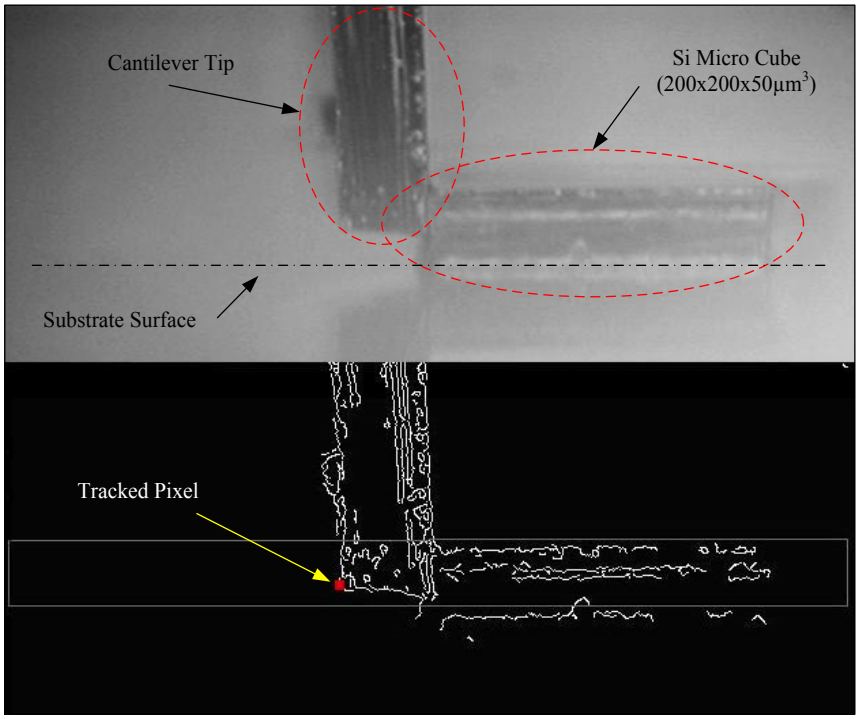

Figure 3-5. Example of a grabbed frame and the edges detected. The highlighted pixel is tracked in all the grabbed frames to obtain the cantilever deflection and applied forces. The rectangular frame outlines the pixel search zone for the algorithm.

3.3.3 Sample Preparation and System Calibration

In this section, two tasks that need to be performed prior to experimental analysis are described: sample preparation and system calibration.

Surface conditions, such as asperities, hydrophobicity, and contaminations due to residue and dust particles, contribute to increasing the impact of micro forces. To assure the cleanness of the surfaces, the following procedure, portrayed in Figure 3-6, is performed to prepare the micro cubes on the substrate for pushing.

i. The process begins by picking up micro cubes with different sizes from the gel pad, where they are stored and placing them into an acetone bath (Figure 3-6a and Figure 3-6b). This task is carefully conducted using an ultra fine tweezers under stereomicroscope.

ii. Each micro object is agitated and moved around in the acetone bath by tweezers to assure the gel clusters are completely dissolved in the acetone solution from all sides of the micro cube.

iii. The surface of substrate is rinsed in acetone.

iv. To clean the acetone residue form the surfaces, both the object and substrate are rinsed first by Isopropyl alcohol (IPA) and then by distilled water.

v. After the surfaces dry, the micro objects are placed on the substrate with a separation distance of roughly 1mm from each other to allow for the pushing process (Figure 3-6c). Touching and gripping micro cubes by tweezers are performed very gently at this stage to prevent scattering the silicon debris from the fragile edges of the silicon micro objects on the substrate.

vi. The substrate and micro object surfaces are rigorously examined under a high-zoom (X800) optical microscope. In spite of the aforementioned cleaning procedure, a few particles usually remains on the surface at this point. A wet contamination (which is probably a thick mix of gel and acetone) is observed on the surfaces of a few micro cubes (Figure 3-6d).

vii. The particles which are located along or in the vicinity of the pushing path are removed individually by a 5μm tip.

viii. A small piece of lens cleaning tissue is attached to the tip to clear the contamination from the top surfaces (Figure 3-6e). The micro object is then flipped over to clean the opposite side of the micro object.

Figure 3-6f signifies one of the micro cubes after the cleaning process is complete.

A system calibration is also necessary to enhance the signal-to-noise ratio. Too stiff a cantilever means too small a deflection, and is not resolvable by the camera. On the other hand, using an excessively compliant cantilever results in a deflection too large to fit in the camera's field of view (FOV). Considering this criterion, the lengths of the cantilever are calibrated with different stiffness values to measure three different ranges of the required pushing force, listed in Table 3-1.

Each time the cantilever is exchanged and before collecting results, a few dry runs of pushing the micro objects are performed to eliminate any possible mechanical drift in the cantilever. To eliminate any errors caused by thermal drift, all the electrical components of the system are turned on at least half an hour before the start of the testing.

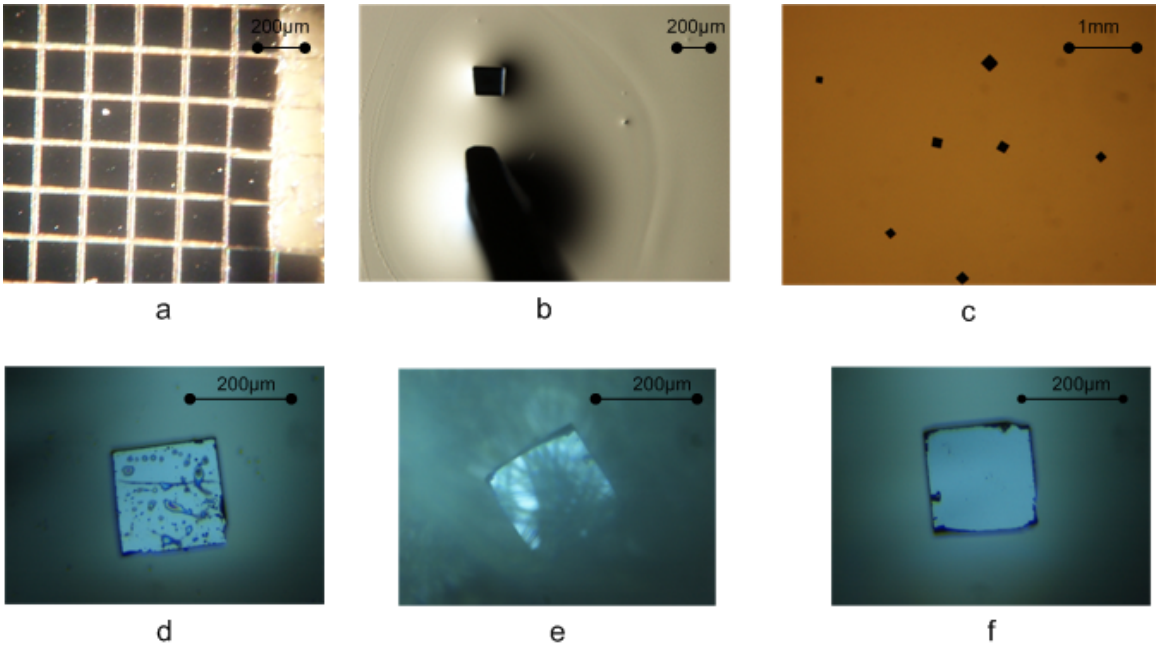

Figure 3-6. Snapshots of the micro objects in the process of cleaning: (a) micro objects are stored on a gel pad, (b) micro objects are rinsed in acetone and IPA using an ultra fine tweezers, (c) micro objects are placed on the substrate after being rinsed in acetone and IPA, (d) a wet viscous contamination on the surface of a micro object, (e) the surface of the micro objects are cleared by lens cleaning tissue, and (f) a clean micro object.

The principal major uncertainty of the micro forces measurement is in detecting the edge of the cantilever by the vision algorithm. The edge detection error in the experiment is ±2 pixels, or ±1.7 µm, as listed in Table 3-2. Therefore, for the longest cantilever in Table 3-1, the maximum force measurement error in the experiments is ±0.37 µN. Given the magnitude of the micro forces measured by using this cantilever (800 -1100 µN), the force measurement error is as low as 0.05% which is unarguably negligible. For the cantilever with the highest stiffness the micro forces measurement error in a worst-case scenario (the magnitude of the micro forces of 5 µN) is approximately 0.28%. This does not take into account any errors associated with the uncertainties in the elasticity modules of silicon and the measurements of the cantilever dimensions.

3.4 Results

In the micro object pushing experiment system, in Figure 3-4, the stage is moved with different constant velocities to push the object against the cantilever. Then, the actual displacement and velocity of the

object are obtained after compensating for the beam deflection. The parameters such as the velocity of pushing, size of the micro object, substrate material, temperature, and relative humidity are altered, and then the experiments are repeated. What follows presents the data and discusses some of the characteristics of the micro forces according to the experiments.

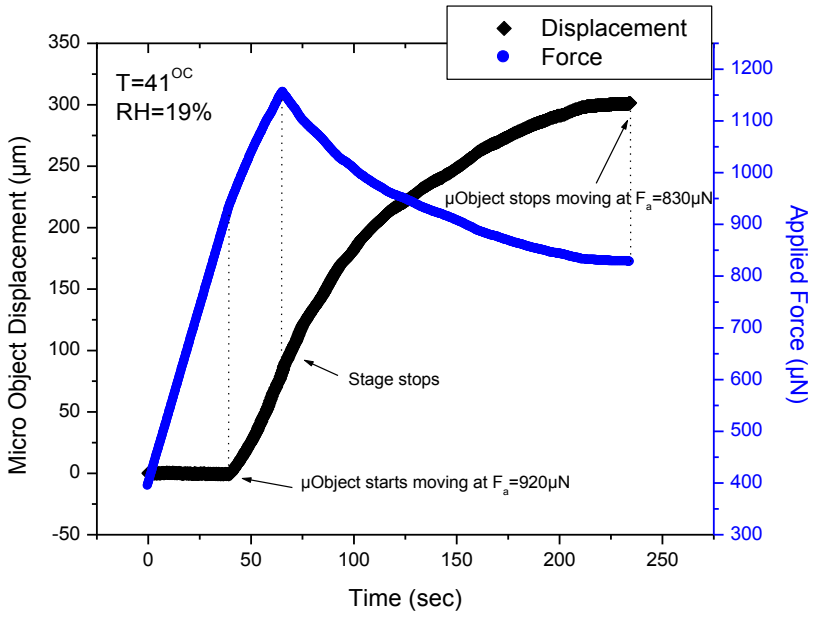

Figure 3-7. Actual trajectory of the micro object and the corresponding applied pushing force, where the 200μm by 200μm by 50μm micro object is placed on an ITO-coated glass.

3.4.1 Static and Kinetic Micro Forces

One of the resultant motion trajectories and the corresponding applied force are plotted in Figure 3-7. The micro object is a cube with a surface size of 200μm x 200μm which is placed on an ITO-coated glass. The object is under a pre-applied lateral force of 400μN before the stage begins to move at t=0 with v=8.9μm/sec. The stage then stops at t=66s, but the energy stored in the deflected cantilever continues to push the μcube for more than 150sec, as it releases its energy. The micro cube's maximum speed is 4μm/sec. In this figure, two types of micro forces are encountered: i) static and ii) kinetic micro forces. The static micro forces are equivalent to the static friction in the macro scale, and occur when the object is not moving with respect to the substrate. Kinetic or dynamic micro forces are measured when the object is

moving. The magnitude of static micro forces in the given ambient conditions is around 920μN whereas that of the kinetic micro forces is as low as 830μN in the plot. The experiment is repeated four times and the variation of the static and kinetic micro forces is about 5%.

3.4.2 Viscous Micro Forces

Figure 3-8 plots the applied forces by the cantilever in relation to the real velocity of the micro objects for pushing a flat micro object of 200μm x 200μm x 50μm on ITO-coated glass at the ambient condition indicated in the graph, which is slightly different from the one in Figure 3-7. The magnitude of the surface forces increases as the velocity increases. This stems from the viscosity that is inherent in micro surface forces such as capillary forces. For velocities ranging from 0.5μm/s to 4μm/s, the force-velocity relationship is almost linear. When the object velocity reaches 4μm/s, however, the viscosity becomes so predominant that the object cannot undergo any velocities higher than 4μm/s regardless of how much lateral force is exerted on the object. The phenomenon is observed in all the scenarios of pushing the objects but the maximum velocity is different at different operational conditions as seen in Figure 3-9 and Figure 3-11. For the plot in Figure 3-8, the data collection stopps when the cantilever deflection goes beyond the camera's FOV at 1150μN, but the aforementioned phenomenon is clearly illustrated in Figure 3-9 and Figure 3-11.

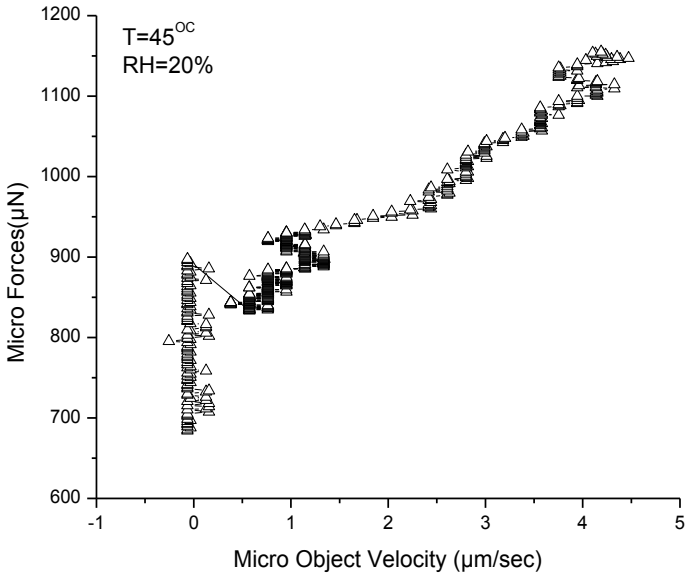

Figure 3-8. Viscous characteristics of micro forces. Data collected in pushing a flat micro object of 200μm x 200μm x 50μm on ITO-coated glass. Maximum object speed is 4 μm/sec.

If more force is exerted at the maximum achievable speed, the micro object, at some point, breaks the bonding with the surface and "skids" away. Figure 3-9 depicts this scenario. The micro object in this plot begins to move at the applied force of 85μN. Although the lateral force is increased by creating more cantilever deflection, the object remains at an average speed of 1.3μm/s. As seen in the plot, the exerted force of 180 μN leads to the micro object breaking the bonding with the substrate, and shooting away to the speed of 7μm/s, momentarily. Most often, the micro object does not immediately land back on the surface and is lost. That is due to the fact that there is almost a zero gravitational force in the normal direction, compared to the high lateral force, such that the object immediately falls down on the substrate after it suddenly loses contact. Therefore, when a micro object is moving at its maximum speed, the application of a higher lateral force must be avoided or the object shoots away and be lost. Figure 3-9 denotes one of the few cases where the micro object quickly resumes its bonding with the substrate, because the object remaines in touch with the cantilever after the momentary skid.

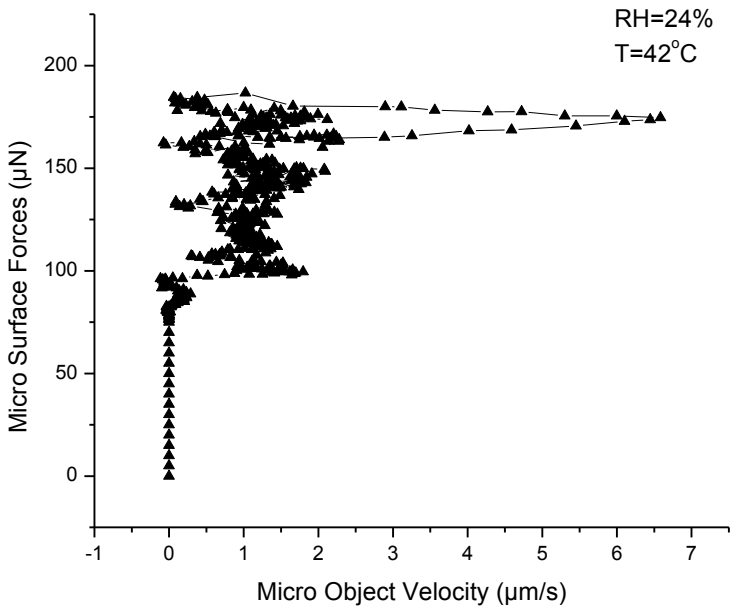

Figure 3-9. Shooting a 120μm x 120μm x 50μm flat micro object during the pushing process on the silicon substrate.

3.4.3 Scale Speed

The scale speed, defined according to (3.1), for pushing flat micro size objects is in the range of 0.002 Hz to 0.030 Hz for all the pushing experiments. For example, for the micro object pushing associated with Figure 3-8, the scale speed is 0.020Hz. This value is 0.011, 0.004, and 0.017 Hz for the pushing scenarios in Figure 3-9, Figure 3-11a, and Figure 3-11b respectively. These numbers are the lowest scale speed among all of the other moving objects listed in Table 3-3. The low scale speed, associated with micro object pushing, suggests that pushing a flat micro object on a flat substrate has an extremely low productivity during the manipulation.

3.4.4 Stick-slip Micro Forces

One of the intrinsic characteristics of micro object pushing is the stick-slip phenomenon which is caused by the changes in the magnitude of the micro forces during the pushing operation. The differences between the static and kinetic micro forces, local surface contamination, or surface alteration are the

primary sources of the changes in the magnitude of the micro forces during the pushing. The highly oscillatory plots in the velocity characteristics of the motion, depicted in Figure 3-8, Figure 3-9, and Figure 3-11, demonstrate the stick-slip characteristics of motion in pushing the micro objects. For example, in Figure 3-11a, the object travels with an average speed of 0.55µm/s. The instant velocity, however, varies between 0.2 and 1µm/s. The instance when the object comes to a full stop, and then slips again is also labelled in Figure 3-11.

Table 3-3. Comparison of scale speed in different object scales[1].

Object	Maximum speed achieved (m/s)	Size of moving object in the direction of motion (m)	Scale speed (s^{-1})
Human running	10.3	0.2	51.5
Human skating	13	0.2	65
Cheetah	30	1.3	23
Tortoise	0.11	0.3	0.36
Garden snail	0.015	0.01	1.5
Horsefly	4	0.007	571
Racing car	115	4.5	25.5
Water boat	142	8.22	17.3
Aircraft	980	32.74	30
Linear macro actuator	10	0.10	100
Flat micro object pushing	6e-6	200e-6	**0.02 - 0.03**

3.4.5 Effects of the Ambient Conditions

To examine the effect of temperature, a heater is used inside the chamber to increase the temperature. Several pushing experiments of different micro objects are conducted at five different temperatures: 24±0.5, 28±1, 34±1.5, 42±2.2 and 54±3^{o}C. Also, the value of the relative humidity, corresponding to the temperature values, is measured. When the moisture content in the enclosure does not change, the relative humidity decreases as the temperature increases. This relationship is shown in Figure 3-10. The experiments in this thesis reveal that the ambient conditions play a significant role in the magnitude of the surface micro forces. In the enclosure with a constant amount of moisture, as the temperature increases from 24^{o}C to 55^{o}C, the magnitude of the static micro forces declines by 35% - 45%, and the maximum pushing speed increases by 350% - 450%. Figure 3-11 denotes the plots obtained from pushing a 150µm x 150µm x 50µm micro object, along the same line on the silicon substrate at two different temperatures.

[1] Data presented are approximated values extracted from [87-90].

By increasing the temperature from 27°C to 57°C, the magnitude of the micro forces decreases by 37% from 135μN to 85μN, whereas the pushing speed increases by 400% from 0.6μm/s to 2.4μm/s.

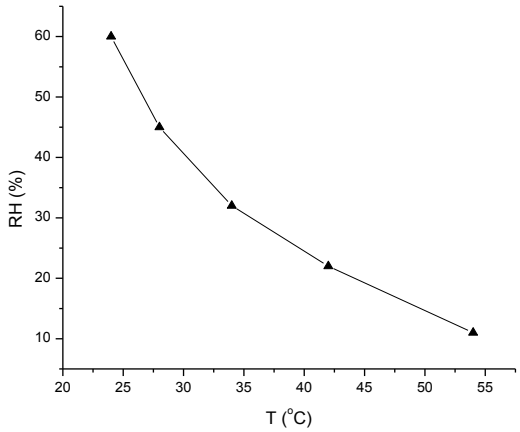

Figure 3-10. Relative humidity inside the enclosed chamber when the temperature increases and the moisture content is invariable. The experiments are conducted at five different temperatures.

Very similar results are illustrated in Figure 3-12 for a 200μm x 200μm x 50μm micro object. The 3-D plots in this figure have been obtained from the micro forces vs velocity plots, similar to those depicted in Figure 3-11. In this figure, more intermediate points are presented, which demonstrate a continuous, up to a 40%, decrease in the magnitude of the micro forces, and a continuous, up to 400%, increase in the pushing speed, when the temperature rises from 24°C to 53°C.

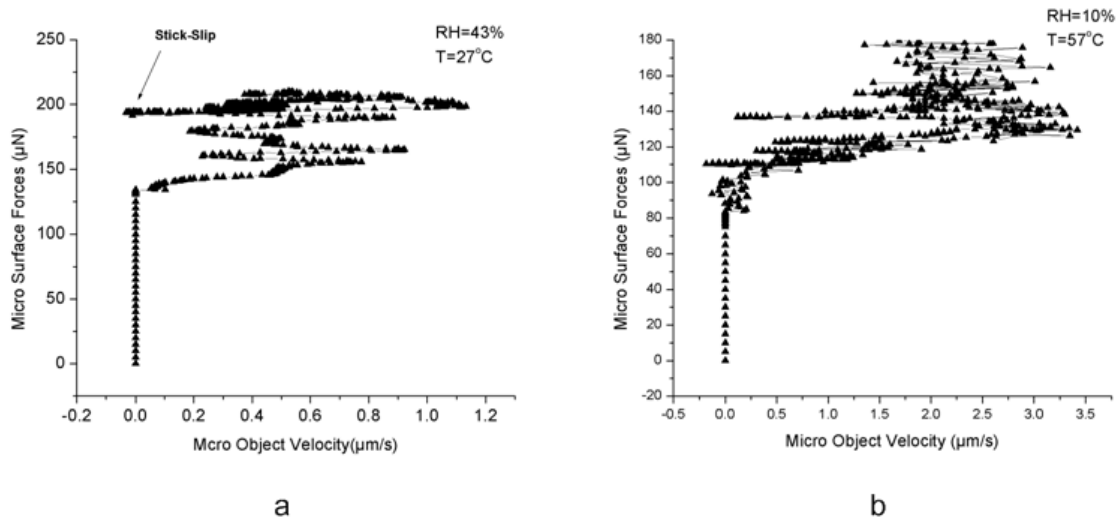

Figure 3-11. Micro surface forces vs velocity in pushing a flat 150µm x 150µm x 50µm micro object on a silicon substrate when the temperature increases inside the chamber with a constant moisture.

In Figure 3-13a, the value of the relative humidity is kept constant at 33% while allowing the temperature to increase. This is performed by injecting more moisture into the chamber as the temperature increases. The results of the magnitude of the micro forces in this scenario differ dramatically from the scenario when no moisture is added to the chamber; the overall magnitude of the micro forces at 57^{o}C is fourfold higher, compared to that obtained at 24^{o}C. Looking at the intermediate stages, however, reveals that this is not a linear increase trend. At high temperatures, the trend is reversed and is similar to that when no moisture is added, that is, the magnitude of the micro forces reduces, when the temperature increases from 37^{o}C to 57^{o}C, while moisture is continuously added to the chamber to keep the relative humidity unchanged at 33%. The decline of the magnitude of the micro forces is 50% at this range of temperature. On the contrary, the magnitude of the micro forces dramatically increases, when the temperature increases from 28^{o}C to 37^{o}C and more moisture is allowed into the chamber. The fact that, at high temperatures, the moisture in the interfacial layer has a much lower viscosity than at low temperature plays a key role in this phenomenon. Nevertheless, a deep understanding of the underlying principles of what is illustrated in Figure 3-13 requires more investigation and experimentation which is beyond the scope of this work.

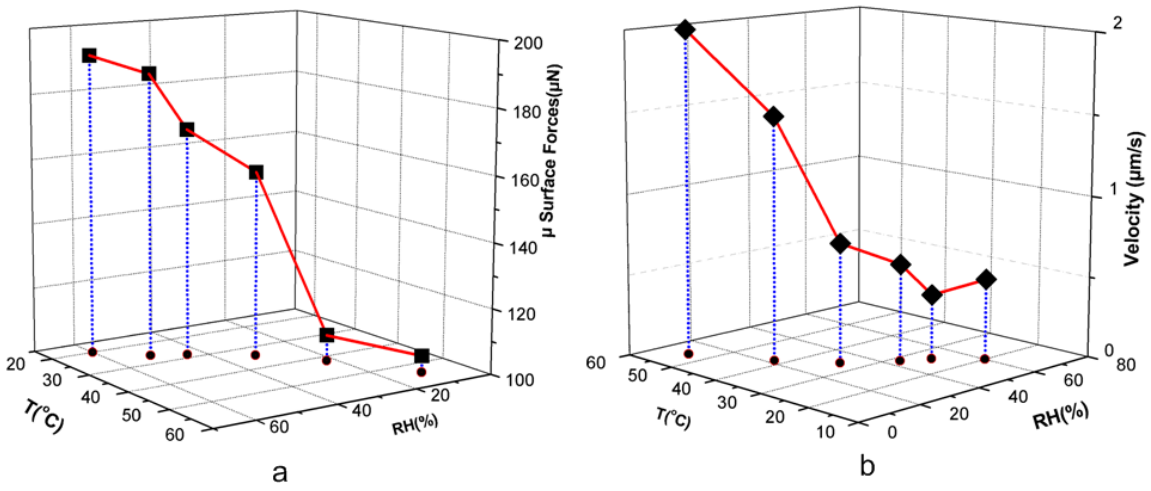

Figure 3-12. (a) Static micro forces, and (b) and maximum velocity in pushing a flat 200μm by 200μm micro object on the silicon substrate at different temperatures when the moisture content is fixed in the enclosure.

Figure 3-13b represents pushing a 200μm x 200μm x 50μm micro object on a silicon substrate, while the temperature inside the chamber is left unchanged and the relative humidity is increased by increasing the moisture content in the chamber. The experiment is repeated three times at each relative humidity to ensure the repeatability of the data. As seen in Figure 3-13b, the magnitude of the micro forces first reduces by more than 50% when moisture is continuously added to the chamber at the fixed temperature. This occurs when the relative humidity increases from about %28 to 46%. During this period, the interfacial layer between the micro object and substrate is relatively dry and increasing the relative humidity can be viewed as the creation of a liquid bridge that serves as a lubricant. Therefore, an increase in the humidity of a dry atmosphere leads to a decline in the magnitude of the micro forces in this range. The trend is opposite when the relative humidity surpasses 50%; the magnitude of the micro forces increases from 125μN at RH=46% to 400μN at RH=77%. This increase is attributed to the formation of large capillary forces in the interface for the high relative humidity values.

3.4.6 Effects of the Size of the Interface Area

Figure 3-14 conveys the effect of the surface area on the magnitude of the micro forces present in this area. The surface area, presented along the x axis is associated with micro objects of sizes 100μm x 100μm, 120μm x 120μm, 150μm x 150μm and 200μm x 200μm, all with a thickness of 50 μm (Table 3-1). As expected, the magnitude of the surface micro forces is linearly proportional to the size of the area.

Measurements are carried out on four to six different micro objects of each size category to assure the repeatability of the data. All the collected data are illustrated in Figure 3-14.

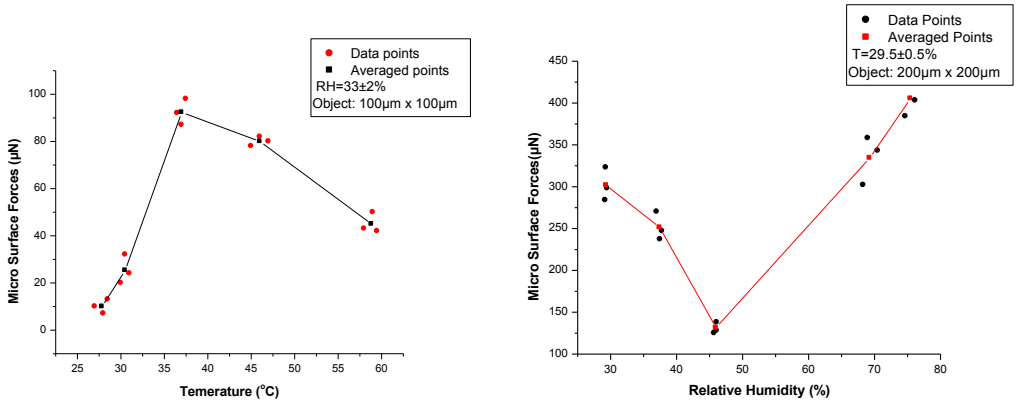

Figure 3-13. The effects of the temperature when the relative humidity is kept constant (left) and the effects of the relative humidity when the temperature is kept constant (right) on the static micro forces in pushing flat micro objects on the silicon substrate. The line connects the average of three data points.

3.4.1 Effects of the Hydrophilicity of the Substrate

In ambient air, a thin layer of water meniscus is formed on the surfaces. The shape and thickness of this layer depends on the degree of hydrophilicity which plays an important role in the magnitude of the micro forces as observed in (2.2). The hydrophilicity of these two surfaces is examined by looking at the shape and curvature of a droplet of water disposed gently by a dropper. Although the thin native oxide layer on the silicon substrate increases the hydrophilicity of the surface, as shown in Figure 3-15, the droplet of water tends to spread out thinner on the ITO-coated glass than the native oxide-coated silicon substrate. This observation is in agreement with the experiments, where the magnitudes of the micro forces on the ITO-coated substrate, illustrated in Figure 3-8, are significantly higher than that on the silicon substrate, evident in Figure 3-12 and Figure 3-14.

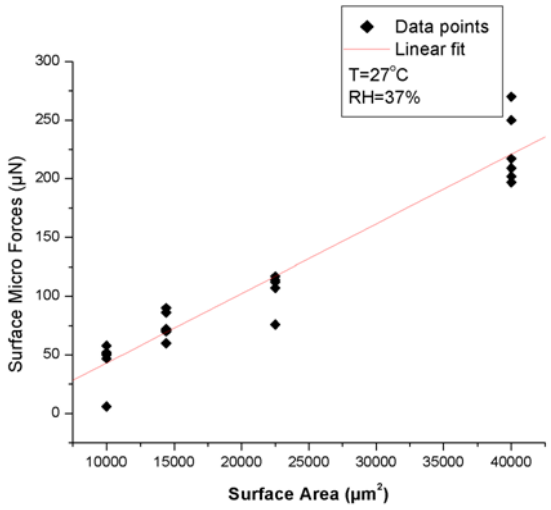

Figure 3-14. The micro surface forces are linearly proportional to the surface area.

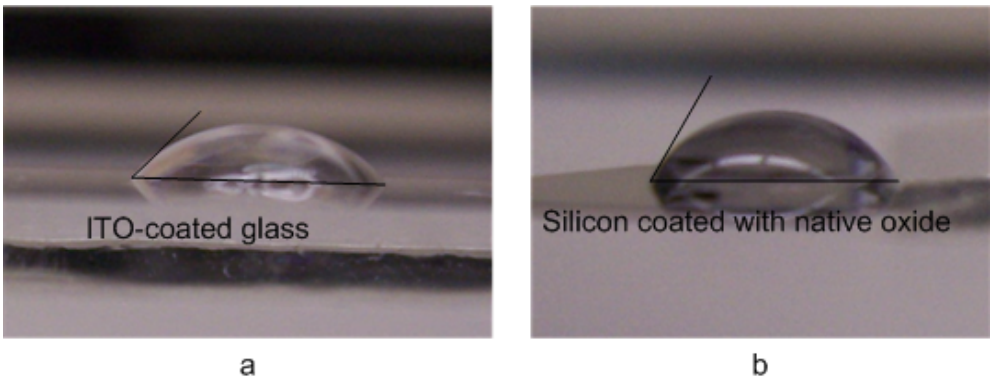

Figure 3-15. The hydrophilicity of the two substrates used in the experiments.

Chapter 4

Design and Implementation of the Adaptive NN-based Controller

4.1 Introduction

In this chapter, a novel approach for the controlled pushing operation of micro size object along a desired path is introduced. The challenges, associated with this control task due to the presence of dominating micro forces are carefully studied, and a solution based on the application of artificial NN is introduced. A nonlinear controller is proposed for the controlled pushing of micro objects which guarantees the stability of the closed loop system in the Lyapunov sense. An experimental setup is designed to validate the performance of the proposed controller through the positioning micro objects.

4.2 Control Strategy

Consider the block diagram in Figure 4-1 where a micro object is sitting on a glass which is, in turn, placed on a micro-stepper-motor-driven stage. A silicon cantilever tip is fixed from one end and is tangent to the side of the micro cube from its other end without any deflection. The x axis of the stage is resting in its origin. To push the micro object, we send the new position command X to the micro stage position controller. The micro stage motion moves the micro object against the micro tip, thus "pushing" the micro object along the x axis. The motion of the micro object is formulated as

$$m\ddot{q} + f_{mf} + F_d = K_s X \quad , \qquad (4.1)$$

where f_{mf}, F_d, , m and $\ddot{q}$ are the micro forces in the contact area, disturbance, mass and acceleration of the micro object, respectively, and K_s is the spring constant of the cantilever. The term, f_{mf}, which is also referred to as the surface micro forces, is affected by parameters such as surface roughness, temperature, humidity, velocity, applied force, geometry of the surface, materials, and electrostatic charge. This makes it extremely challenging to derive a model for this surface force. Unlike the case of conventional macro manipulation systems, this force is considerably large in comparison to the well-known gravitational force resulting from the mass, and cannot be treated as a negligible term. Also, the micro forces are dominant in micromanipulation, and therefore, cannot be incorporated into the disturbance, F_d, in (4.1). Therefore, it is

advantageous to define a learning mechanism which can be trained to fairly estimate this force under varying operating conditions.

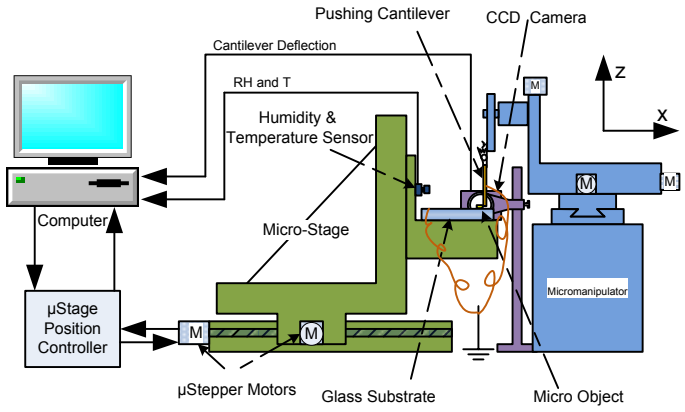

Figure 4-1. Block diagram of the experimental setup.

In Chapter 2, we described a comprehensive investigation to bring together all the influential parameters necessary to determine the overall micro surface force. This force can be represented as a function of the following variables:

$$f_{mf} = f(\dot{q}, F_a, \phi) \ , \qquad (4.2)$$

where $\dot{q}$ is the velocity of the two surfaces in contact, F_a is the applied force, and ϕ is a vector of the environmental parameters, defined as follows:

$$\phi = \phi(R_{ms}, RH, T, E_s, \upsilon_s, E_o, \upsilon_o, m, A). \qquad (4.3)$$

R_{ms} represents the surface roughness in micro scale, RH is the relative humidity, T is the temperature, E_s and υ_s are Young's modulus and the Poisson ratio of the substrate, E_o, υ_o and m are Young's modulus, Poisson ratio, and mass of the micro object, respectively and A represents the surface area in contact.

Surface roughness, R_a , is a measure of the texture of a surface and is defined in the macro scale as an arithmetic average of the surface profile altitude which is measured by using a profilometre [85]. In the micro displacement of micro objects, however, a more suitable measure of the surface topography is desired to define the dominant micro forces, locally at a given place on the substrate. Such a parameter

should be a function of the location on the surface and the conventional R_a. Thus, the roughness in the micro scale is defined by

$$R_{ms} = \Re(R_a, q) \quad , \qquad (4.4)$$

where q is the position of the micro object on the substrate. For simplification, the environmental parameters, which are unlikely to vary during the pushing process, are omitted as input variables in (4.3). Thus, considering (4.4), the micro forces input parameter in (4.2) and (4.3) is re-defined as

$$f_{mf} = f(q, \dot{q}, F_a, \phi) \ , \ \phi = \phi(RH, T) . \qquad (4.5)$$

4.2.1 Neural Networks Controller Design

In order to design a NN-based controller for micro object pushing, the error dynamics of the manipulator are first considered. For the adaptive control of a manipulator, an auxiliary filtered tracking error signal is often required to remove the acceleration components from the dynamic equations.

Here, a novel stable NN controller design, based on filtered error dynamics, is proposed to control a micromanipulator. The control design guarantees the Uniform Ultimate Boundedness (UUB) of the closed-loop system in the Lyapunov sense. Also, the convergence of the tracking error is guaranteed.

Given the desired position trajectory, the tracking error and its derivative are

$$e = q_d - q$$

and

$$\dot{e} = \dot{q}_d - \dot{q} .$$

The filtered tracking error is expressed as

$$r = \dot{e} + ke \ , \qquad (4.6)$$

with $k > 0$. By differentiating (4.6) and invoking (4.1), it is seen that the pushing dynamics can be described in terms of the filtered tracking error as

$$m\dot{r} = kmr + f_{mf}(q, \dot{q}, F_a, \phi) + F_d - K_s X + m\ddot{q}_d - k^2 me. \qquad (4.7)$$

The NN control law can be defined as

$$X = \frac{1}{K_s}[\hat{f}_{mf}(q, \dot{q}, F_a, \phi) + k_v r + m\ddot{q}_d - k^2 me], \qquad (4.8)$$

where $\hat{f}_{mf}$ is an estimate of f_{mf}, and $k_v r = k_v \dot{e} + k_v k e$ is an outer PD tracking loop.

4.2.2 Neural Networks Approximation

According to the universal approximation property of NN [84], there exists a two-layer NN such that

$$f_{mf}(q, \dot{q}, F_a, \phi) = W^T \sigma(V^T x) + \varepsilon \ , \qquad (4.9)$$

where the weight matrices, W and V, are unknown parameters that are tuned online during pushing processes. These ideal target weight matrices are not necessarily unique. The approximation error is bounded on a compact set by $\varepsilon \le \varepsilon_N$, with ε_N a known bound.

The activation function σ at the hidden layer is a nonlinear function (typically a sigmoid function) given by

$$\sigma(x) = \frac{1}{1 + \exp(-x)}. \qquad (4.10)$$

Since the size of the NN is difficult to determine, the weight estimates of $\hat{W}$ and $\hat{V}$ are often used with a certain size to approximate the function,

$$\hat{f}_{mf}(q, \dot{q}, F_a, \phi) = \hat{W}^T \sigma(\hat{V}^T x) \ . \qquad (4.11)$$

Then, the following weight estimation errors are defined as

$$\tilde{W} = W - \hat{W} \ , \ \tilde{V} = V - \hat{V}. \qquad (4.12)$$

The functional approximation errors can be defined as

$$\tilde{f}_{ms} = f_{mf} - \hat{f}_{mf} \quad , \qquad (4.13)$$

and the hidden layer output error is described as

$$\tilde{\sigma} = \sigma - \hat{\sigma} \quad , \qquad (4.14)$$

where $\sigma = \sigma(V^T x)$ and $\hat{\sigma} = \sigma(\hat{V}^T x)$ and its Taylor series expansion about $\hat{V}^T x$ is

$$\sigma = \hat{\sigma} + \sigma'(\hat{V}^T x).(\tilde{V}^T x) + \mathrm{O}(\tilde{V}^T x)^2$$

$$\Rightarrow \tilde{\sigma} = \sigma'(\hat{V}^T x).(\tilde{V}^T x) + \mathrm{O}(\tilde{V}^T x)^2 \ . \qquad (4.15)$$

4.2.3 Training Algorithm

To prove the stability of the control law in (4.8) for pushing micro objects in the presence of dominant micro forces, several assumptions and conditions are outlined in this section.

4.2.3.1 Assumption 1 (Bounded Reference Trajectory):

The desired pushing trajectory is bounded such that

$$|q(t)| \le q_B \ , \ |\dot{q}(t)| \le \dot{q}_B \ , \ |\ddot{q}(t)| \le \ddot{q}_B, \qquad (4.16)$$

where $q_d, \dot{q}_d, \ddot{q}_d$ are the desired trajectory, velocity, and acceleration, respectively, and $q_B, \dot{q}_B$, and $\ddot{q}_B$ are known scalar bounds.

4.2.3.2 Lemma 1 (Bound on Neural Networks Input, x):

For each time, *t*, the NN input vector, *x(t),* is bounded.

Proof: the NN input vector x, according to (4.5) is

$$x = [q \ \dot{q} \ F_a \ \phi] = [q \ \dot{q} \ F_a \ RH \ T]^T \ . \qquad (4.17)$$

The applied force is the potential energy stored in the cantilever due to the deflection during the pushing process. If Δl is the cantilever's deflection, then the applied force is expressed as

$$F_a = K_s \Delta l = K_s (X - q) \ . \qquad (4.18)$$

By substituting from (4.8)

$$F_a = \hat{f}_{mf} + k_v r + m\ddot{q}_d - k^2 me - K_s q$$
$$= \hat{f}_{mf} + k_v r + m\ddot{q}_d - k^2 me - K_s (q_d - e)$$

Therefore, the NN input vector x in (4.17) is

$$x(t) = [(q_d - e) \quad (\dot{q}_d - r + ke) \quad (\hat{f}_{mf} + k_v r + m\ddot{q}_d - k^2 me - K_s q_d + K_s e) \quad RH \quad T]^T$$

The humidity and temperature are bounded by a constant (= $c_1 > 0$). Since the NN activation function (sigmoid) is bounded, the NN output parameter is also bounded, that is, $\hat{f}_{mf} \le c_2$. Therefore,

$$|x(t)| \le c_1 + c_2 + (1 + K_s) q_B + \dot{q}_B + m\ddot{q}_B + (1 + k + k^2 + K_s)|e| + (1 + k_v)|r| . \quad (4.19)$$

Since $k \ge 0$, it can be derived from the solution of (4.6) that

$$|e| \le |e_0| + \frac{|r|}{k} \quad (4.20)$$

where $e_0 = e(t_0)$ is the initial tracking error at the start of the pushing. Then, the bound can be expressed as

$$|x(t)| \le c_1 + c_2 + (1 + K_s) q_B + \dot{q}_B + m\ddot{q}_B + (1 + k + k^2 + K_s)|e_0| + (2 + k + k_v + \frac{1 + K_s}{k})|r| . \quad (4.21)$$

Therefore, the NN input vector is bounded, as long as the controller guarantees that the filtered tracking error $r=r(t)$ is bounded.

Since the tracking error is bounded according to (4.20), and the mass of micro size objects is extremely small, compared to the tracking error and estimated scaling forces, the terms, $m\ddot{q}_d - k^2 me$ are negligible and omitted from (4.5).

4.2.3.3 Theorem 1 (Weight Updating Rule)

Consider the dynamic system of the micromanipulator, described by (4.7), for the bounded, continuous desired trajectory with bounded velocity and acceleration. The NN controller, (4.8), guarantees the UUB of the close-loop system with the gains satisfying $k_v - km > 0$, and the NN weight tuning algorithms given by

$$\begin{cases} \dot{W} = M\hat{\sigma}r \\ \dot{V} = Nx(\hat{\sigma}'^{T}\hat{W}r)^{T} \end{cases}, \qquad (4.22)$$

where M and N are the constant positive definite matrices. Moreover, the weight estimates, $\hat{W}$ and $\hat{V}$ are bounded and the filtered tracking error, r, drops to zero asymptotically.

***Proof**:* By substitution of (4.11) in (4.18), the control signal is

$$X = \frac{1}{K_s}[\hat{W}^{T}\sigma(\hat{V}^{T}x) + k_v r + m\ddot{q}_d - k^2 me] \quad . \quad (4.23)$$

Now, by substitution of (4.23) and (4.9) into the error dynamics (4.7) and using the estimation errors in (4.12), (4.13), and (4.14), one obtains:

$$m\dot{r} = (km - k_v)r + W^{T}\sigma - \hat{W}^{T}\hat{\sigma} + (\varepsilon + F_d) \qquad (4.24)$$

Adding and subtracting $W^{T}\hat{\sigma}$ yields

$$m\dot{r} = (km - k_v)r + \tilde{W}^{T}\hat{\sigma} - W^{T}\tilde{\sigma} + (\varepsilon + F_d) \quad . \quad (4.25)$$

By adding and subtracting $\hat{W}^{T}\tilde{\sigma}$ in (4.25)

$$m\dot{r} = (km - k_v)r + \tilde{W}^{T}\hat{\sigma} + \hat{W}^{T}\tilde{\sigma} + \tilde{W}^{T}\tilde{\sigma} + (\varepsilon + F_d)\,.$$

By substituting the (4.14),

$$m\dot{r} = (km - k_v)r + \tilde{W}^{T}\hat{\sigma} + \hat{W}^{T}\hat{\sigma}'\tilde{V}^{T}x + \omega(t) \quad , \quad (4.26)$$

where

$$\omega(t) = \tilde{W}^{T}\hat{\sigma}'\tilde{V}^{T}x + W^{T}\mathrm{O}(\tilde{V}^{T}x)^2 + \varepsilon + F_d$$

is called the disturbance term. The pushing disturbance, F_d, NN approximation error, ε, and the higher order terms in the Taylor series expansion, all have the same weights as the disturbance in the error system.

Several conditions must be imposed on the error system in (4.26).

Condition-1: k should be positive definite.

Condition-2: Weights (W and V) and activation function, σ, should be bounded.

Condition-3: The first derivative of the activation functions should be bounded as well.

To satisfy the last two conditions, the sigmoid function is a good candidate because this function and its first differentiation are both bounded by unity.

Define the Lyapunov candidate as

$$L = \frac{1}{2}mr^2 + \frac{1}{2}tr(\tilde{W}^T M^{-1}\tilde{W}) + \frac{1}{2}tr(\tilde{V}^T N^{-1}\tilde{V}) \quad . \qquad (4.27)$$

By differentiating the above equation and substituting from (4.26) yields

$$\dot{L} = r[(km - k_v)r + \tilde{W}^T\hat{\sigma} + \hat{W}^T\hat{\sigma}'\tilde{V}^T x]$$
$$+ tr(\tilde{W}M^{-1}\dot{\tilde{W}}) + tr(\tilde{V}^T N^{-1}\dot{\tilde{V}})$$

For the sake of simplicity, it is assumed that the influence of the disturbance, $\omega(t)$, is negligible. Since

$$r\tilde{W}^T\hat{\sigma} = tr(\tilde{W}^T\hat{\sigma}r)$$

and

$$r\hat{W}^T\hat{\sigma}'\tilde{V}^T x = tr(\tilde{V}^T xr\hat{W}^T\hat{\sigma}') \ ,$$

$$\dot{L} = -(k_v - km)r^2$$
$$+ tr\{\tilde{W}^T(M^{-1}\dot{\tilde{W}} + \hat{\sigma}r)\} \qquad . \qquad (4.28)$$
$$+ tr\{\tilde{V}^T(N^{-1}\dot{\tilde{V}} + xr\hat{W}\hat{\sigma}')\}$$

Since W and V are constants, $\dot{\tilde{W}} = -\dot{\hat{W}}$, $\dot{\tilde{V}} = -\dot{\hat{V}}$. If the tuning algorithm (4.22) holds, the last two terms in the right hand side of (4.28) would become zero, and

$$\dot{L} = -(k_v - km)r^2 .$$

The parameter $(k_v - km)$ is consistently positive as long as the gains of the outer PD tracking loop satisfy $k_v > km$. This leads to $\dot{L} \le 0$, and since $L > 0$, the stability in the sense of Lyapunov (SISL) is deduced. Moreover, by considering (4.20), the boundedness of all the terms in the right hand side of (4.7), and consequently the boundedness of $\dot{r}$ can be concluded. As such, $\ddot{L} = -2(k_v - km)r\dot{r}$ is bounded, and thus, $\dot{L}(t)$ is uniformly continuous. By applying Barbalat's Lemma [81], it is evident that $\dot{L}(t)$ should approach zero as t goes to infinity. As a result, the filtered tracking error, $r=r(t)$, vanishes.

4.3 Design of the Experimental Setup

This section provides details about the proposed system and the experiments conducted to validate the performance of the controller developed in the previous section. The goal of the experiment is pushing a micro size cube from point "A" to point "B" on a substrate along a desired trajectory with the highest possible precision. The degree of the positioning accuracy achieved by the well-known proportional-integral-derivative (PID) controller is often sufficient for a linear system. However, it is well known that micro forces are extremely nonlinear. As a result, a PID controller might not achieve the desired performance in the presence of micro forces during the controlled micro pushing. Therefore, in this section, the impact of implementing a NN-based controller for micromanipulation in pushing tasks is investigated. Also, the position accuracy of this method is compared with that of conventional filtered tracking error-based PD controller [86].

4.3.1 Hardware Setup

The experimental setup is depicted in Figure 4-1, and its hardware specifications are listed in Table 4-1. A micro object is placed on a glass which is, in turn, placed on a micro-stepper-motor-driven stage. A silicon cantilever tip is fixed from one end and pushes the micro object from its other end. To push the micro object, the stage is allowed to move the micro object against the micro tip, making the necessary contact and moving the micro object along the x axis.

To visually track the micro cube and micro tip and to capture the camera frames of the pushing process, a high-definition CCD camera mounted on a high magnifying zoom lens is installed next to the stage, aligned along y axis. The camera is connected to a personal computer via a video acquisition board, where programs with the Graphical User Interface (GUI) are run. Attached to the microstage is a humidity-temperature sensor which monitors the ambient conditions in real time. After the humidity and temperature data are collected, they are fed into the GUI program.

Table 4-1. List of hardware specifications.

Hardware	Specification
Micro stage	Translational resolution: 0.156µm Velocity resolution: 0.745µm/sec
Vision system (CCD Camera + lens)	Resolution: 0.85µm/pixel Field of view: 640 x 480 pxls=545 x 415µm
Temperature sensor	Resolution: 0.1 Celsius degrees

Relative humidity (RH) sensor	Resolution: 0.1%
Micro cube	Dimensions: L200 × W200 × Thk50 µm Diced out of 50 µm Thick DSP Si Wafer
Micro cantilever	Dimensions: L16300 × W200 × Thk50 µm Diced out of 50 µm Thick DSP Si Wafer Stiffness: 0.217706 µN/µm
Glass substrate	Coated with Indium Tin Oxide (ITO)

To minimize the effect of the electrostatic charges during the pushing operation, the ITO-coated glass substrate and the cantilever are wired to a common ground. Figure 4-2 portrays the entire system housed in an enclosure and placed on a vibration-isolated optical table. The horizontally applied force vector undergoes about 8º change of angle due to the cantilever's deflection. To account for this deflection during pushing, the cantilever is inclined according to Figure 4-2d by 4º. This inclination is intended to keep the effective pushing force horizontal throughout the experiment.

4.3.2 Controller and Software Design

The proposed NN-based control strategy is incorporated into a generic program with GUI. This program facilitates the automated 1-D pushing of any micro size object, along any desired trajectory in which the position is a monotonically increasing function of time.

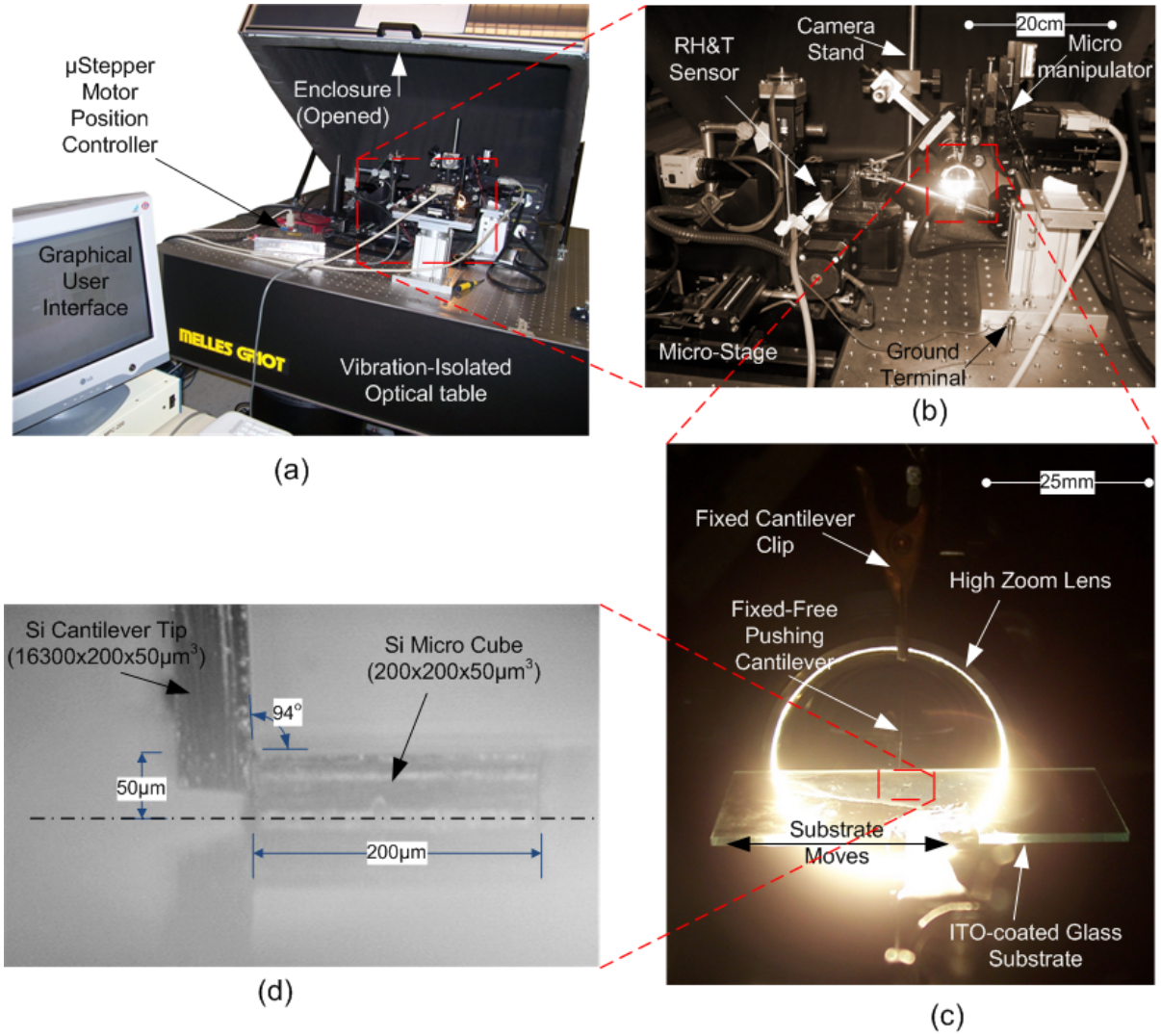

Figure 4-2. Experimental setup for controlled micro object pushing: (a) the entire hardware setup. The enclosure is closed during the controlled pushing experiment to help stabilize the ambient conditions inside, (b) hardware configuration including the micro stage, micromanipulator, camera, and temperature-humidity sensor placed on the grounded optical table, (c) the 200µm-wide slim cantilever is vertically supported from its upper end by the clip. The clip is clamped to the micromanipulator. The micro cube lies on the glass substrate which is supported on the position-controlled micro stage, and (d) a high-zoom frame at the start of the pushing. The cantilever is angled by 4º to retain the effective applied force horizontal during the pushing. The blurry reflection of the micro cube and cantilever tip are seen in the substrate.

Automated micro object pushing can be carried out in one of two fashions: *i)* open-loop and *ii)* closed-loop. The open-loop controller merely neglects any elastic deformation imposed on the cantilever tip by the resisting micro forces. A block diagram of this approach is shown in Figure 4-3a. The closed-loop controller is a visual-servo mechanism which utilizes the real time information of the actual position of

the micro cube to compensate for the cantilever deflection. To this end, two different types of closed-loop controllers are investigated in this thesis; the conventional linear PD controller in Figure 4-3b, and the proposed NN-based nonlinear controller in Figure 4-3c. The NN-based controller is the application of the control law in (4.8), which is designed to ensure tracking and UUB stability in the Lyapunov sense.

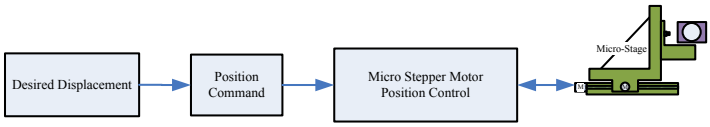

(a) Open loop controller

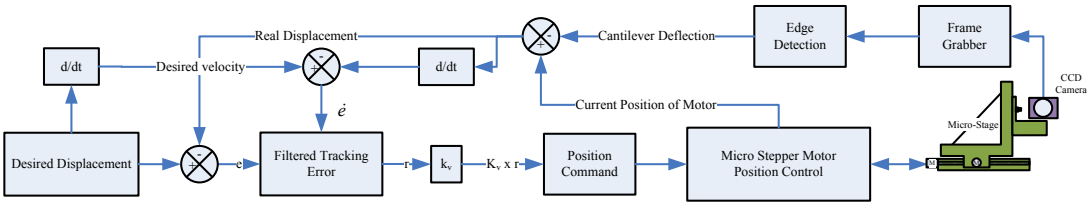

(b) Linear closed loop controller

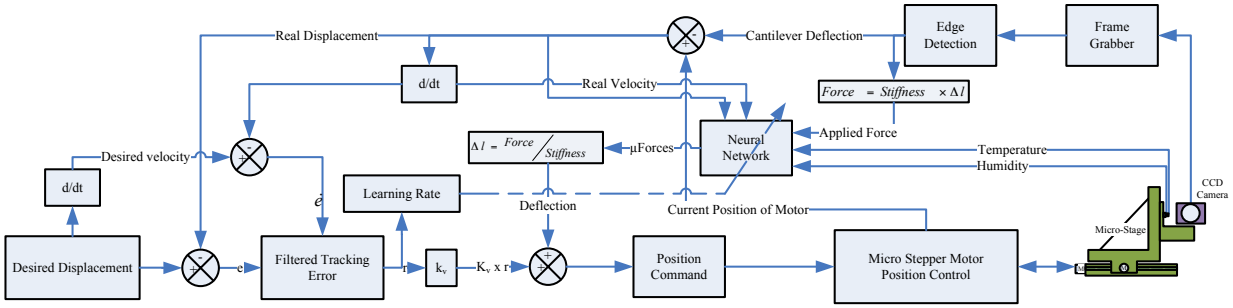

(c) Proposed non-linear adaptive NN-based controller

Figure 4-3. The micro object pushing controllers designed with different strategies.

The weight matrices of the NN are tuned in two manners: *i)* off-line back-propagation training [82] and *ii)* dynamic learning during pushing by using (4.22). The former is known as supervised learning (requires training data) or static NN, whereas the latter is called unsupervised learning or dynamic NN. Details of the training algorithms in both cases are discussed in the next sections.

The real position of the micro object in the feedback controlled pushing operation is measured visually in this experiment. The grabbed frames from the CCD camera are fed into an image processing program to detect the edges of the micro cube and the cantilever. We adopt the canny edge detection algorithm available from open source OpenCV libraries for this application. The parameters of the canny algorithm designed for the visual servo movement in the experiment are listed in Table 4-2.

Table 4-2. List of software specifications.

Real time data acquisition frequency	2Hz
Edge detection algorithm	cvCanny High threshold:900 Low threshold: 450 Sobel kernel size: 5
PD controller parameters [Filtered tracking $k_v r = k_v(\dot{e} + ke)$]	$k_v = 0.2$ k=5
Unsupervised NN learning rate	M=0.0005 , N=0
Maximum measurement error of real position (edge detection error)	±2pxl = ±1.70 μm
Microstage velocity threshold	v ≤ 7.5 μm

As seen in Figure 3-5, the deflection of the cantilever can be calculated according to this pixel location. Consequently, given the exact position of the micro-stepper motor-driven stage at any time instant, the real displacement of the micro cube is calculated in real time by using this method. The experiments demonstrate a very reliable measurement of real displacement of the object by using this algorithm.

4.3.3 Artificial Neural Network Structure

Equation (4.5) defines five distinct variables contributing to the magnitude of the micro forces at any given instance. These parameters, forming the input vector to the NN, are position, velocity, applied pushing force, temperature, and humidity. In the absence of any mathematical model, the proposed two layer feed forward NN model (4.11) outputs the approximate value of the nonlinear micro forces described in (4.5). Table 4-3 lists the parameters that define the structure and size of the NN. These parameters are defined by a trial-and-error process.

4.3.4 Sample Preparation and System Calibration

In this section, two necessary calibration procedures that need to be performed prior to the experimental analysis are described. First, surface conditions such as the asperities, contamination by residue and dust particles, and hydrophobicity contribute to increasing the impact of micro forces. Acetone is used as a solvent to remove all the contamination of the surface of the glass substrate and micro cubes. To clean the acetone residue, both object and substrate are first rinsed in Isopropyl alcohol (IPA) and then by distilled

water. This procedure is performed in a clean room environment, and the surfaces are rigorously examined under a high-zoom (X800) optical microscope.

Table 4-3. NN size and structure.

Number of inputs	5
Neurons in hidden layer	10
Number of outputs	1
Data sets for training	370
Data sets for testing	50

Secondly, to enhance the signal-to-noise ratio, the stiffness of the cantilever is calibrated. Too stiff a cantilever means too small a deflection, not resolvable by camera; on the other hand, using an excessively compliant cantilever results in a deflection too large to fit in the camera's FOV. Considering this criterion, the length for the cantilever is selected through a trial-and-error process and is 16.3mm.

4.3.5 Data Gathering and Processing for Control Design

Prior to the automated pushing process, the behaviour of the developed system is characterized by implementing multiple runs of open-loop pushing. In what follows, the procedure for selecting the control parameters is described.

4.3.5.1 Desired Pushing Trajectory

It is known in control engineering applications that not any arbitrary response can be achieved in practice due to physical and hardware constraints. For example, in macro manipulation, it is often unsafe to run a robot arm at a speed higher than a velocity threshold. Such limitation also applies in micromanipulation. The difference, however, is that safety is usually not an issue due to the negligible inertia in the micro scale. Instead, the experiments show that the so-called viscous behaviour of the micro forces dictates the maximum achievable micromanipulation speed. This stems from the scaling effect of the adhesion due to the capillary present in the interface between the micro object and the substrate. Figure 4-4 illustrates the layer of moisture which surrounds the micro cube, forming a capillary force.

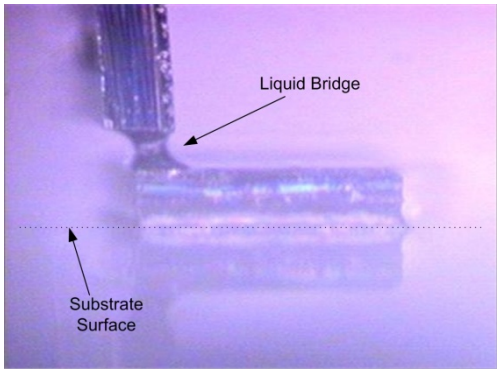

Figure 4-4. Capillary force in micro object pushing. Touching on and retracting back from the surface by the tip magnifies the existence of a moisture layer as the tip adsorbs them from the upper side of the µcube to form a big liquid bridge. An unseen moisture layer also exists on the bottom side of the µcube.

In the controlled pushing experiment, the stage is moved with different velocities to push the object against the cantilever. Then, the actual velocity of the object displacement is obtained after compensating for the beam deflection. One of the resultant motion trajectories and the corresponding applied force are plotted in Figure 4-5. In this figure, two types of micro forces are encountered: i) static and ii) kinetic micro forces. Static micro forces are equivalent to the static friction in the macro scale, and occur when the object is not moving with respect to the substrate. The Kinetic or dynamic micro forces are measured when object is moving. The magnitude of static micro forces is approximately 920µN, whereas those of the kinetic micro forces are as low as 830µN in this plot. As inferred from the plot in Figure 4-5, the kinetic micro forces also exhibits viscous behaviour when the micro cube is moving with different speeds.

Figure 4-5 plots the forces applied by the cantilever when the object is moving at different velocities and the stage is moving at a constant velocity of 8.9µm/sec. The magnitude of the micro forces indicates a nonlinear behaviour with respect to the velocity. It is evident that the magnitude of the micro forces strikingly increases at a pushing speed beyond 4µm/sec. This information leads to setting the maximum desired velocity of the object below 4µm/sec (3.8µm/sec in the selected desired trajectory).

Based on these observations, a sinusoidal desired trajectory is selected for pushing as illustrated in Figure 4-7. This trajectory captures different pushing velocities over time, and is, therefore, a suitable choice for gathering the data to train the ANN and optimize the network weights to better approximate f_{mf} in (4.9).

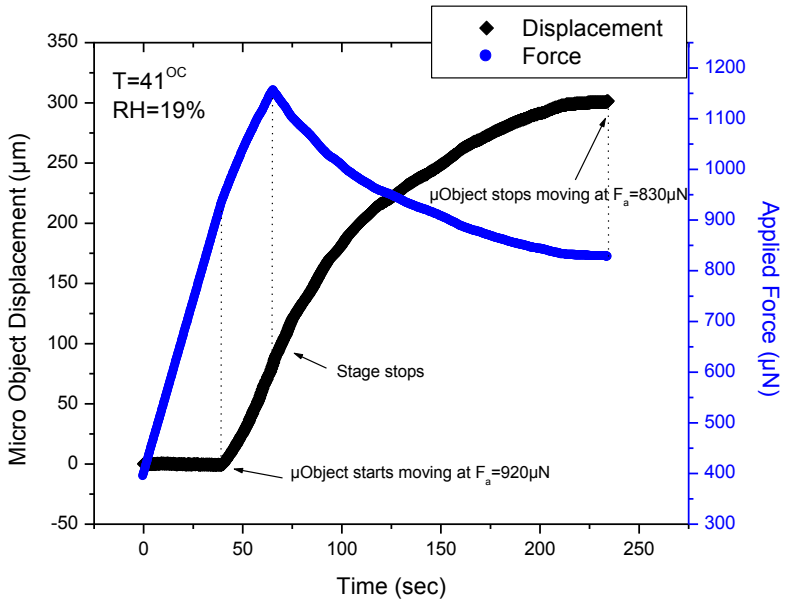

Figure 4-5. Open-loop pushing of the micro cube. Micro stage starts moving at *t=0* with *v*=8.9μm/sec and stops *at t=66s*. Then, the energy stored in deflected cantilever keeps pushing the μcube for more than 150sec as it releases its energy. The micro cube's maximum speed is 4μm/sec. The dynamic micro forces is shown to be about 10% less than the static micro forces.

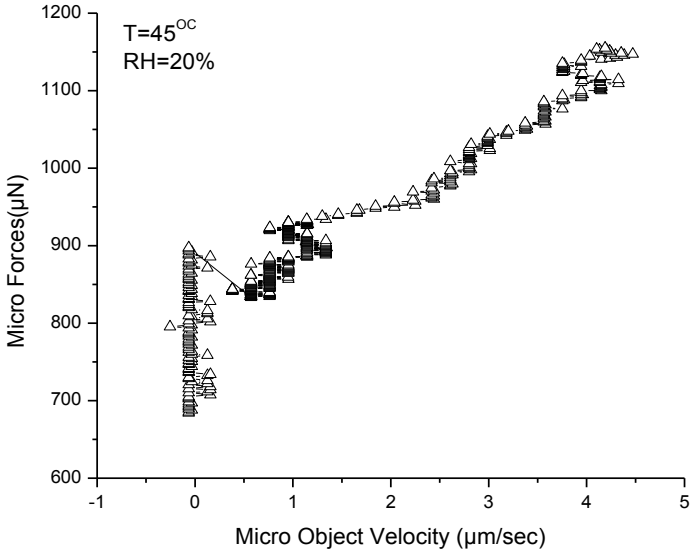

Figure 4-6. Saturation of the pushing speed and the force-velocity data points collected in the micro cube pushing, when the stage moves with a constant velocity of 8.9μm/sec.

4.3.5.2 Static Neural Network Weights Tuning

About 370 data features are used to train the feed forward multilayer NN. The training is conducted by using a back propagation algorithm [82]. The input of each data set is that from (4.17). The output is micro forces, f_{mf} . Fifty more data sets are also used to test the performance of the trained NN. The training and test data are collected from the various plots of the micro forces in relation to the applied force, velocity and real position. These plots are indirectly extracted from the data gathered during a series of pushing experiments, performed at fixed ambient conditions, temperature and humidity, along a fixed line on the substrate. The fact that the absolute position of the micro cube on the glass is among the NN input data is an important implication that the network is being trained for a particular positioning path.

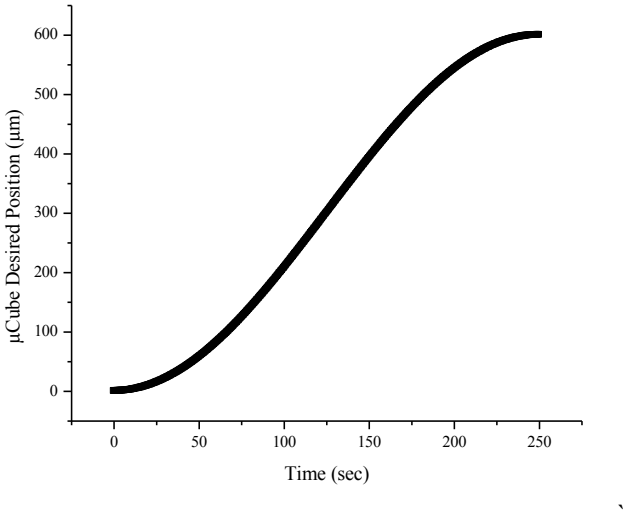

Figure 4-7. Sinusoidal trajectory for pushing.

Figure 4-8 reflects a subset of the data in a 3-D surface representation. Axes x and y represent the absolute position and velocity of the micro object, respectively. The z axis corresponds to the "required pushing force" at a fixed applied force, temperature, and humidity. The 430 training and test data features are extracted from a group of similar 3-D surface plots that capture the pushing forces at various positions, velocities, and applied forces and at fixed RH=4% and T=40^{o}C.

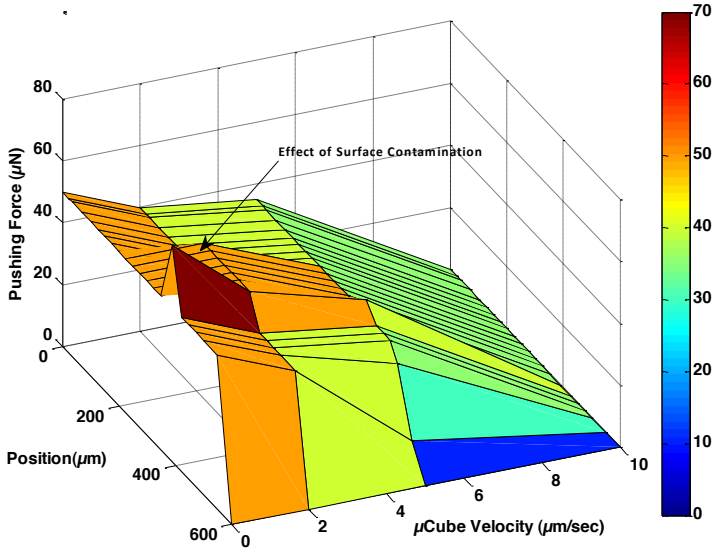

Figure 4-8. Subset of NN input-output training data. F_a=*40μN, RH=4%* and $T=40^{OC}$. The sharp spike at the middle of the position axis is the result of a local contamination on the substrate.

4.4 Results

This section comprises the results of implementing the open loop control method in Figure 4-3a, PD control method in Figure 4-3b and the proposed NN-based controller in Figure 4-3c, for the automated pushing of micro objects along the position trajectory in Figure 4-7. For these experiments, PD control gains are tuned manually to achieve the best possible tracking performance. During the implementation of the NN-based control in Figure 4-3c, the tuned PD gains are kept unchanged to directly examine the impact of adding the NN approximation term in (4.8) and how accurately it can predict the scaling force dominant during the micro object pushing. The NN-based control is implemented in two different ways: i) PD + static NN, and ii) PD + dynamic NN. The former approach utilizes a NN trained off-line using the 370 data features, discussed in Section 4.3.5.2. The data are used to train the NN to approximate the scaling forces based on the input vector x in (4.17). During the controlled pushing, the NN weights are kept static. In approach (ii), the NN weights are allowed to change in real time, according to (4.22), to ensure a better tracking as well as the UUB stability in the Lyapunov sense.

4.4.1 Actual Positioning Plots

Figure 4-9 depicts the position error obtained by pushing a micro cube of the dimensions 200x200x50μm^3 along the trajectory in Figure 4-7. The experiment is carried out at a relative humidity of 4% and a

temperature of 40^{O}C (±0.5% fluctuation) in the enclosure in Figure 4-3a. The micro forces characterization data used to train the static NN are those collected at these ambient conditions based on the approach discussed in the previous section.

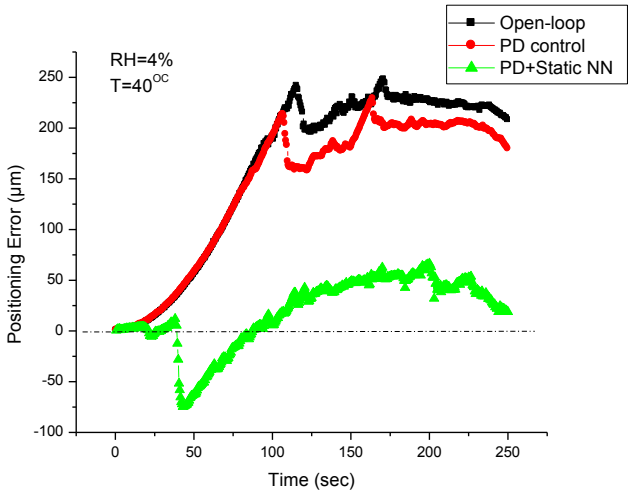

Figure 4-9. Micro cube positioning error with three different controllers, and ambient conditions are kept unchanged.

Figure 4-10 demonstrates the superiority of the NN model in (4.8) adopted to compensate for the un-modelled micro forces, compared to the conventional linear PD controller in Figure 4-3b. The static NN, however, loses its effectiveness gradually over time as the contamination distribution and ambient conditions change. This phenomenon is observed in Figure 4-10 where the static NN performance deteriorates when the humidity changes to 9% and temperature increases slightly to 42°^{C}.

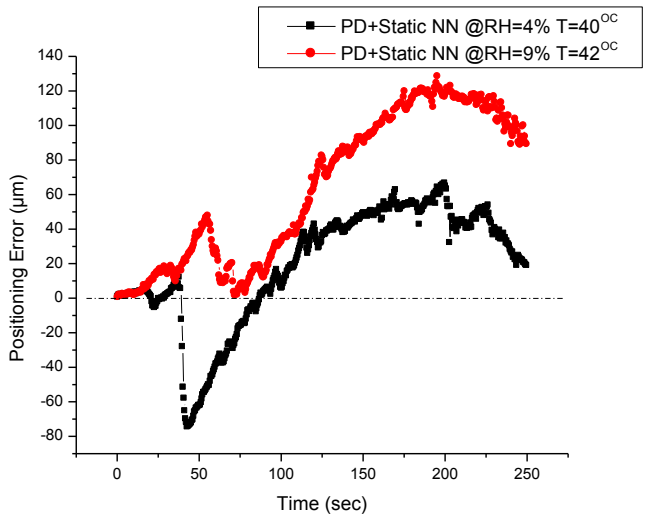

Figure 4-10. Static NN approximation accuracy deteriorates when the ambient conditions are altered slightly.

To allow the NN model to capture the scaling forces in varying operating conditions, dynamic dynamic learning is utilized according to the settings summarized in Table 4-2 and the control architecture in Figure 4-3c. For learning to occur when f_{mf} varies, the pushing operation is repeated sequentially and the updated NN weights at the end of each run are stored and then used to initiate the NN for the next run. The position error of five sequential runs is denoted in Figure 4-11. The adaptive learning process performed by the dynamic NN approach is clearly observed in Figure 4-12, where the Root Mean Square (RMS) error decreases as the trajectory in Figure 4-7 is repeated over and over. The RMS error is calculated for each run as follows

$$E_{RMS} = \sqrt{\frac{1}{n}\sum_{k=1}^{n} e_k^2} \quad , \qquad (4.29)$$

where e_k is the position error at time instant k, and n=500 is the number of data samples acquired experimentally during each run.

The plot suggests that the learning saturates after pushing four times along the same trajectory. More pushing with this learning rate does not significantly improve the positioning accuracy. The RMS error, obtained at the end of learning cycle, reduces to10µm, and the absolute positioning error at the final destination x=600µm is as low as 2µm. Therefore, the proposed control strategy with adaptive learning

considerably improves the accuracy of positioning the micro object, compared with the positioning error obtained by using the PD controller. These results reveal the potential use of the adaptive NN to design stable controllers for accurate and reliable micromanipulation.

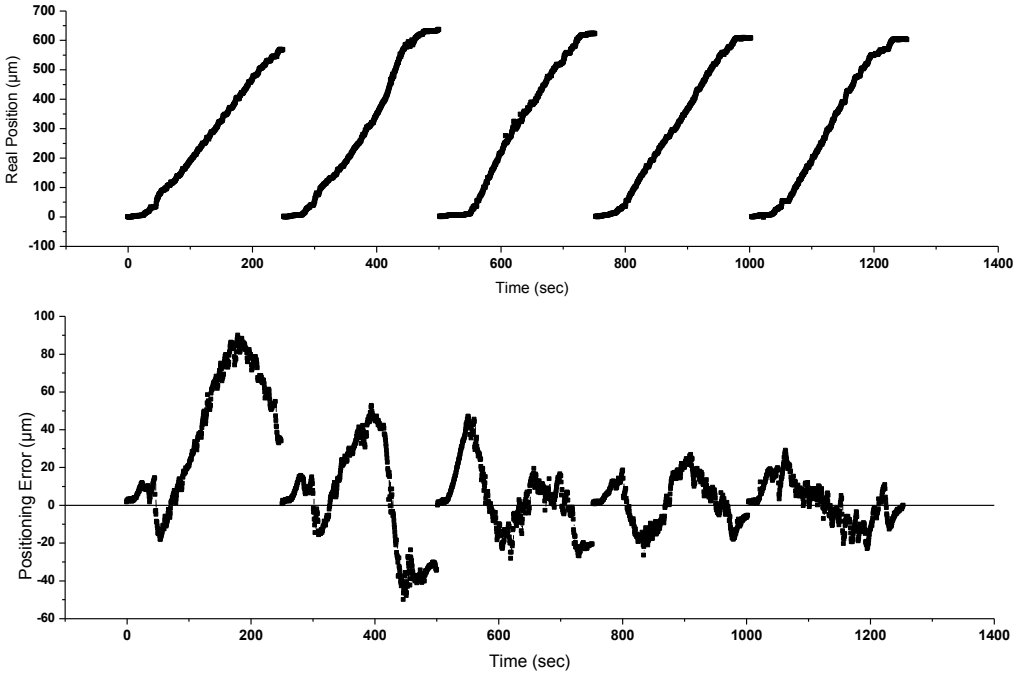

Figure 4-11. Plots obtained from five runs of the pushing micro cube. The first run is performed by the static NN in which no weights are updated in real time. For the next four runs, dynamic NN is used. The NN weights at the end of the previous run are used to re-initialize the NN. The object is brought back to its initial position after each run.

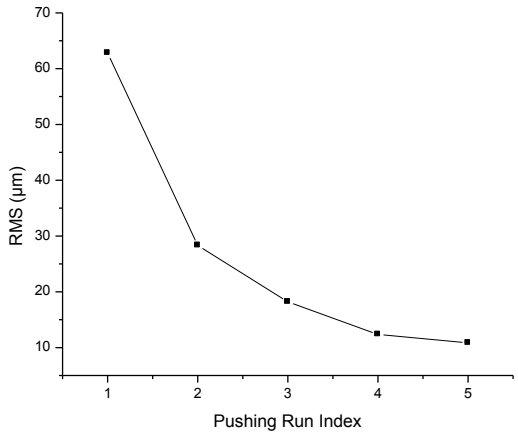

Figure 4-12. RMS error change vs. dynamic NN.

4.4.2 Repeatability of the Results

The pushing experiments in section 4.4.1 are repeated four times to ensure the consistency of the results, as demonstrated in the plots. To account for the non-uniformity in the surface contamination, the object is returned to its initial position after the completion of each push. The RMS errors of each run for various control methods are listed in Table 4-4. The repeatability of the results is obvious from the data recorded in this table.

Table 4-4. Root Mean Square of the positioning error in different pushing strategies.

RMS	**Run 1**	**Run 2**	**Run 3**	**Run 4**	**Average**
Open loop	181.1	188.0	184.4	182.2	183.9
PD	161.3	161.7	163.3	159.5	161.4
PD + static NN @RH=4% T=40^{OC}	39.2	37.3	42.7	44.2	40.8
PD + static NN @RH=9% T=42^{OC}	61.0	60.9	70.4	58.9	62.8

Chapter 5

Automated Sequential Micromanipulation

5.1 Introduction

In the previous chapter, a control system was experimentally demonstrated for the automated positioning of a single flat micro object accurately along the desired trajectory. In this chapter, the application of the proposed controller is extended to accurately push several micro objects, each with different characteristics in terms of the surface micro forces governing the manipulation process. This chapter confirms that the proposed adaptive controller is capable of learning to adjust its weights effectively, when the surface micro forces changes under varying surface and ambient conditions.

Accurately positioning several micro objects to a specific target location by microactuators is a common task in an automated microassembly line. The goal of this chapter is to validate the performance of the proposed NN in applications such as sequential microassembly, in which, the automated manipulation of multiple micro components is desired to construct a more complex micro structure. The specifications of the experiments in this chapter follows. Three flat micro components are placed along a line with a separation distance of a few hundred micrometres. The components are fabricated from a silicon wafer but have different dimensions and will be microassembled. A microassembly process is designed to operate according to the following procedures:

i. The micro components are continuously fed to the microassembly line and placed at their initial station.

ii. Each of these components are then accurately pushed and positioned in a target station.

iii. In the target station, another micromanipulator is available to perform the post-pushing manipulation.

In this chapter, the automated sequential pushing of these three micro components from their initial stations to their specific target stations is discussed. The automated operation is with precision even under varying ambient conditions.

5.2 Control Strategy

In the serial manipulation of objects with different sizes, the surface area is no longer constant but varies from one object to the next. Therefore, referring to (4.2) and (4.3), the surface micro forces involved in this process can be expressed as follows,

$$f_{mf} = f(q, \dot{q}, F_a, A, \phi) \quad , \quad \phi = \phi(RH, T) \quad . \quad (5.1)$$

This implies that a new parameter, the surface area, should be added to the input vector of the NN in the proposed controller as described in Chapter 4. Accordingly, in this experiment, the NN control law in (4.8) is modified to the following:

$$X = \frac{1}{K_s}[\hat{f}_{mf}(q, \dot{q}, F_a, A, \phi) + k_v r + m\ddot{q}_d - k^2 me] \quad . \quad (5.2)$$

According to the universal approximation property of NN [82], there exist a two-layer NN such that

$$f_{mf}(q, \dot{q}, F_a, A, \phi) = W^T \sigma(V^T x) + \varepsilon \quad . \qquad (5.3)$$

It is very challenging to find the size of the matrices, W and V, which gives the arbitrary approximation error of ε. Therefore, the weight estimates of $\hat{W}$ and $\hat{V}$, with a certain size are adopted to approximate the function, such that

$$\hat{f}_{mf}(q, \dot{q}, F_a, A, \phi) = \hat{W}^T \sigma(\hat{V}^T x) \quad . \qquad (5.4)$$

The control design follows the same procedure as discussed in detail in Section 4.2.1.

The stability of the controller is proven in Chapter 4. In the controller, employed for sequential pushing in this chapter, the parameter of the surface area is added to the input of the NN according to (5.4). The value of the surface area, determined in the image processing algorithm, is bonded in the largest size of the camera's FOV. Therefore, following the same arguments as those in Section 4.2.3, the UUB of the nonlinear controller for sequential pushing of micro objects with different sizes is guaranteed. Moreover, the filtered tracking error, *r(t),* vanishes over time, similar to the controller discussed in Section 4.2.

5.3 Hardware Setup

In this experiment, the hardware and the system configuration are the same as those in the previous chapter. The only difference is that, instead of having one micro object on the substrate, there are three micro objects lined up with a separation distance.

Figure 5-1 is a schematic of how the objects are initially positioned, as well as the target position after pushing operation.

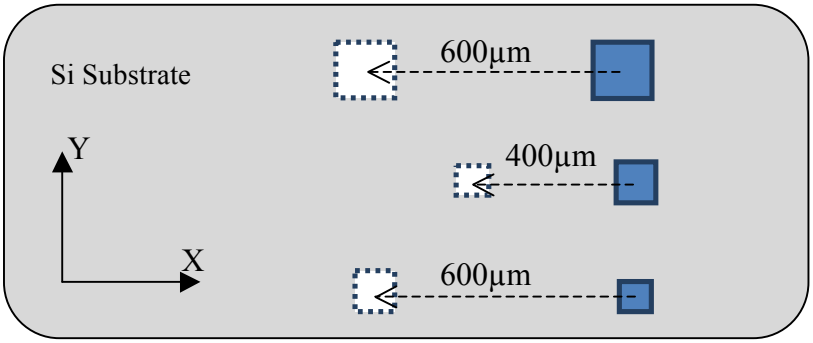

Figure 5-1. Initial and target position of the micro objects during the automated sequential micromanipulation.

The square objects used for this experiment are diced out from a 50 µm thick silicon wafer. The sizes of the objects are 125x125 µm, 150x150 µm, and 200x200 µm. Also, the substrate on which the objects are and the cantilever to push the objects consists of silicon. The cantilever in this particular experiment is 14 mm long, 200 µm wide, and 50 µm thick. The hardware specifications are summarized in Table 5-1.

5.4 Controller and Software Design

The controller used in sequential pushing is similar to the one described in the previous chapter with the following modifications

- The vision system outputs the size of the object in addition to its position on the substrate. The size of the object determines the contact surface area which is one of the input parameters of the NN in the sequential manipulation of the multiple objects with different sizes.

- The automation of the process in realized by integrating an open loop controller with the proposed closed loop controller, described in the previous chapter: The open-loop controller is used during the short time window when the micro stage is moving rapidly to the initial position of the next object. Therefore, no pushing is taking place during this period. The entire process is performed without any operator intervention.

Table 5-1. List of hardware specification.

Hardware	**Specifications**
Micro stage	Translational resolution: 0.156µm Velocity resolution: 0.745µm/sec
Vision system (CCD Camera + lens)	Resolution: 0.85µm/pixel Field of view: 640 x 480 pxls=545 x 415µm
Temperature sensor Relative humidity (RH) sensor	Resolution: 0.1 Celsius degree Resolution: 0.1%
Micro object 1 Micro object 2 Micro object 3	Dimensions: L200 × W200 × Thk50 µm Dimensions: L150 × W150 × Thk50 µm Dimensions: L120 × W120 × Thk50 µm All diced out of 50 µm Thick DSP Si Wafer
Micro cantilever	Dimensions: L14000 × W200 × Thk50 µm Diced out of 50 µm Thick DSP Si Wafer Stiffness: 0.34 µN/µm
Glass substrate	Silicon Wafer

Similar to the the process of single object manipulation in Chapter 4, the experiment is repeated several times with the open-loop controller, PD controller and the proposed NN-based adaptive controller. The block diagrams describing the structure of each of these three controllers are provided in Figure 5-2.

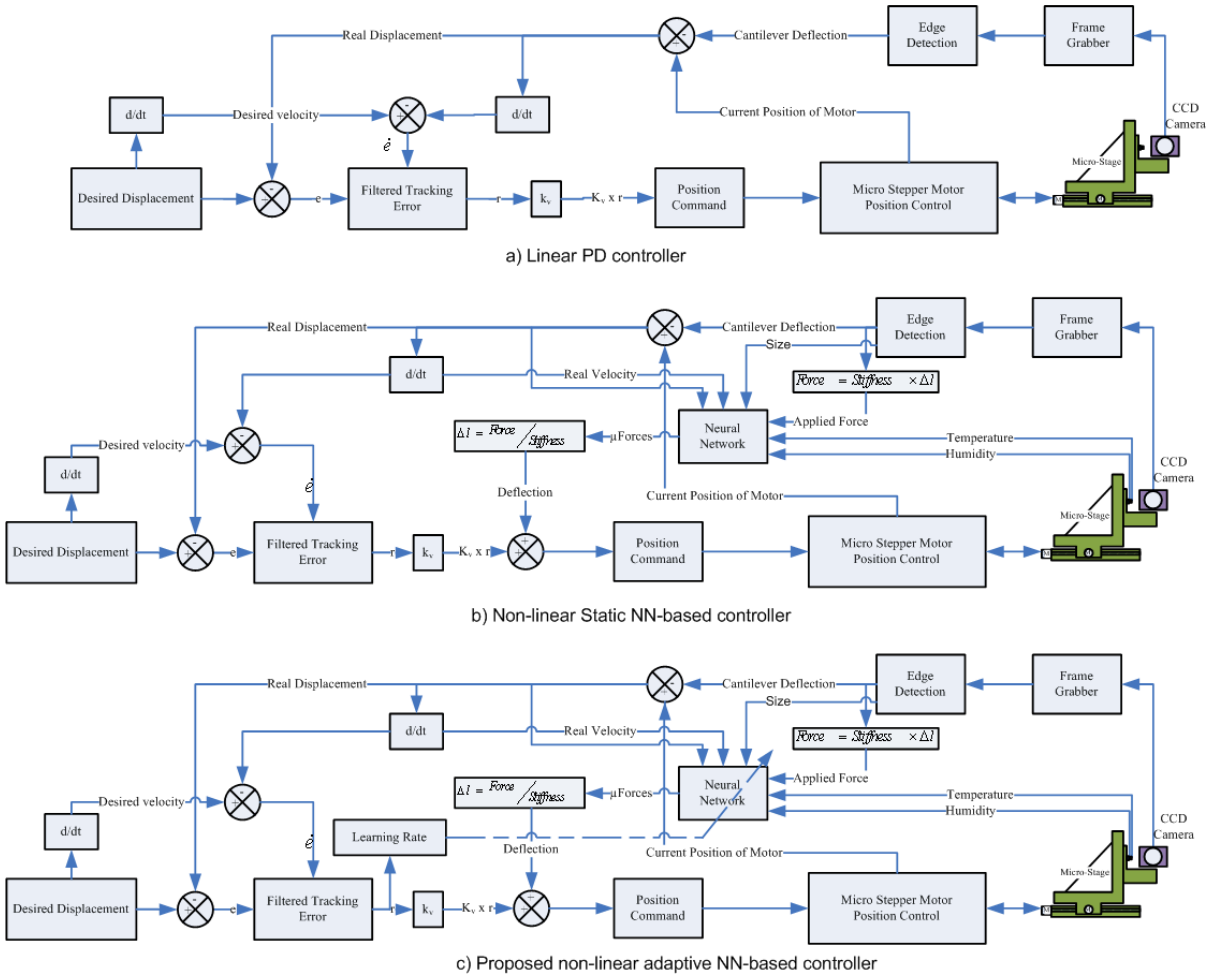

Figure 5-2. Sequential micro object positioning controllers with different strategies.

The description of the proposed software is provided in detail in Section 4.3.2.

5.5 Artificial Neural Network Structure

Equation (5.1) identifies six distinct variables that determine the magnitude of the micro forces at any given instance. These parameters, forming the input vector to the NN, are listed here.

- A: Surface area of the object at the interface with the substrate
- q: Current Position of the micro Object

- F_a: Amount of force being applied on the object
- $\dot{q}$:Velocity that the object is travelling at
- RH: Relative humidity
- T: Temperature of the enclosure

The proposed two layer feedforward NN model in (5.4) outputs the approximate values of the nonlinear micro forces described in (5.1). Table 5-2 lists the parameters that define the structure and size of the NN used in the sequential micro object pushing experiments. These parameters are obtained through a trial-and-error process.

Table 5-2. NN size and structure

Number of inputs	6
Neurons in hidden layer	10
Number of outputs	1

5.6 Sample Preparation and System Calibration

In order to properly clean the objects that are being pushed, the following procedure is necessary:

1. The various objects are picked up by using ultra-fine tweezers from the gel pad on which they are stored, and placed onto an intermediate glass slide which has been cleaned with acetone and wiped dry.
2. With an eye dropper, a few drops of acetone are placed on the objects in order to remove any dirt or other contaminants from the objects. While soaked in acetone, the objects are pushed around on the slide by the ultra-fine tweezers to assist in the removal of these contaminants.
3. Once the acetone is allowed to dry, the previous step is repeated by using isopropyl alcohol (IPA), and again allowed to dry.
4. The surface of the silicon substrate is rinsed with acetone and wiped dry.
5. Under a microscope, the objects are gently picked up from the glass slide by using the tweezers and placed on the newly-cleaned silicon slide.
6. Under the same microscope, the objects are gently pushed to the pre-defined positions through the use of the ultra-fine tweezers. Moving the objects around at this point also helps to remove any dirt that might be trapped between the object and the substrate during the transfer between the slides.

7. The substrate is inspected for dust or any other contaminants that might disturb the tests, and any offending particles are removed under microscope using ulta fine probe tips.

The procedure for cleaning the cantilever is similar to that of cleaning the objects. First, the cantilever is rinsed with acetone and IPA. Then, it is rinsed once more with acetone. The cantilever is then placed in its containing clip and grounded to prevent any stray charges on the surface.

5.7 Desired Pushing Trajectory

Three sinusoidal trajectories are chosen as the desired trajectories of the pushing. The sinusoidal trajectory is smooth and contains different pushing velocities over time and is therefore a suitable choice for gathering the data to train the ANN and optimize the network weights to a better approximate f_{mf} in (5.4). Figure 5-3 depicts the trajectories in relation to the time for the three micro objects. The pushing distance in these trajectories is selected to both satisfy the hardware limitations and demonstrate the effectiveness of the proposed control strategy.

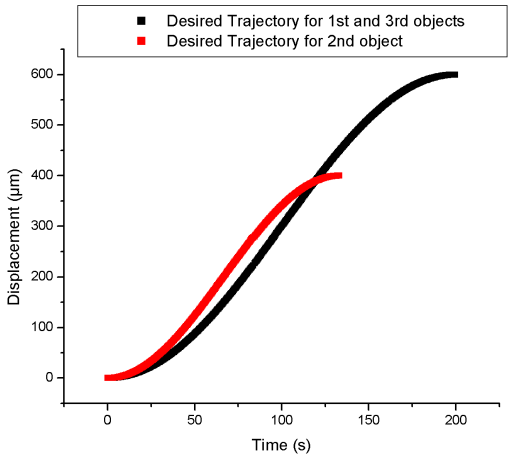

Figure 5-3. Desired trajectories for the sequential automated positioning of the micro objects with different sizes.

5.7.1 Tuning NN Weights

In Chapter 4, a series of open-loop pushing steps are conducted to identify the key characteristics of the micro forces and to prepare enough data sets to train the NN, prior to integrating it into the closed-loop control system shown in Figure 5-2c.

In this chapter, although the micro objects and their surface characteristics are changed, and consequently, the resulting micro forces have considerably different magnitudes, no further characterization of the micro forces is required prior to the automated manipulation. The data sets in Chapter 4 are utilized to create the training sets. The proposed adaptive NN, as demonstrated in the following sections, is capable of quickly adjusting its weights under varying operating conditions by applying the proposed weight tuning algorithm in (4.22).

Several micromanipulation cycles must be run, until the adaptive controller has effectively adjusted its weight to the new condition. After each of these automated sequential micromanipulation cycles are complete, the program outputs an updated W matrix which is a modified version of the original matrix obtained during the static NN training. For the next run of the automated micromanipulation, this new matrix is fed into the program, replacing the previous one as its initial W matrix. This ensures that the program always uses the most accurate data during the micromanipulation process, and, therefore, guarantees continuous learning.

5.8 Results

In this section, the results of sequentially pushing three objects are provided. The objects are initially positioned according to Figure 5-1, and are pushed along the desired trajectory illustrated in Figure 5-3. The sequential micro object pushing is repeated with three different controllers.

i) Conventional PD controller in Figure 5-2a

ii) PD controller, augmented with static NN in Figure 5-2b, and trained as described in Section 5.7.1

iii) The proposed adaptive NN-based controller in Figure 5-2c with weight updates according to (4.22).

In total, seven runs of automated sequential pushing of three micro objects are carried out. The first experiment is conducted by using PD controller for positioning. The second run is performed by adding the static NN to the PD controller. The table of training sets is constructed by using the data obtained in Chapter 4 and according to Section 4.3.5.2.

The experiment is continued by conducting 5 additional cycles of sequential pushing in which the W matrix of the NN is dynamically updated through the experiment according to (4.22). The performance of the control system in each case is reported in the following sections.

The experiments are carried out when the chamber is at the relative humidity (RH) of %52 and temperature is measured 32^{o} Celsius.

5.8.1 Sequential Micromanipulation Using the PD Controller

Figure 5-4 illustrates the results of the automated sequential pushing of the three micro objects on a silicon substrate by using conventional PD controller with the parameters discussed in Table 4-2.

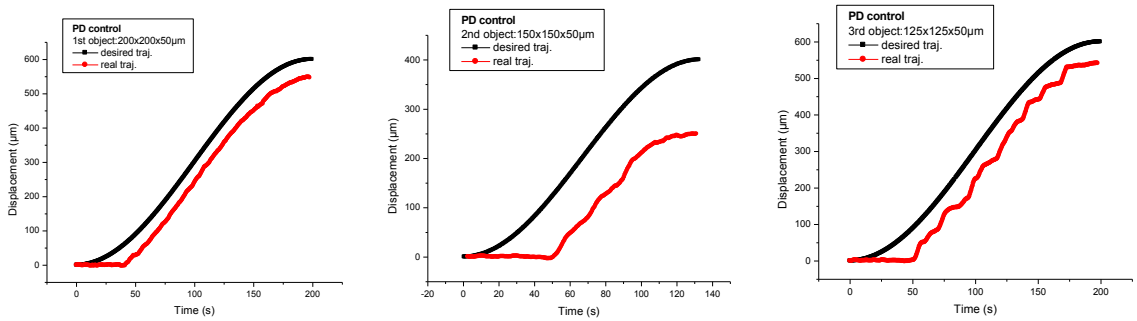

Figure 5-4. Actual trajectories of the micro objects in sequential micromanipulation by PD controller (Run#1).

A stick-slip characteristic is almost always present at the start of the pushing as is clearly seen in the plots. After the pushing has commenced, the micro objects frequently slow down and might completely cease depending on the characteristics of the surfaces. For example, the displacement curve for the third object hits a horizontal line for a period of time on several occasions during the manipulation, demonstrating a stick-slip behaviour of the object. In the case of the second object, the displacement curve suggests that the object slows down on two occasions throughout the pushing process. In contrast, the first object almost smoothly follows the desired trajectory beyond the initial stick-slip phenomenon. The plots in Figure 5-4 verify that the PD controller is incapable of compensating for the non-linear micro forces during the pushing. This is more evident, when the object being pushed exhibits a stick-slip behaviour.

5.8.2 Sequential Micromanipulation Using PD Controller Augmented with Static NN

The sequential micromanipulation of the same three objects, along the same path is repeated by augmenting a NN to compensate for the nonlinear micro forces during the pushing process. The NN is trained according to the procedure described in Section 5.7.1. In Figure 5-5 the performance of this control system is demonstrated.

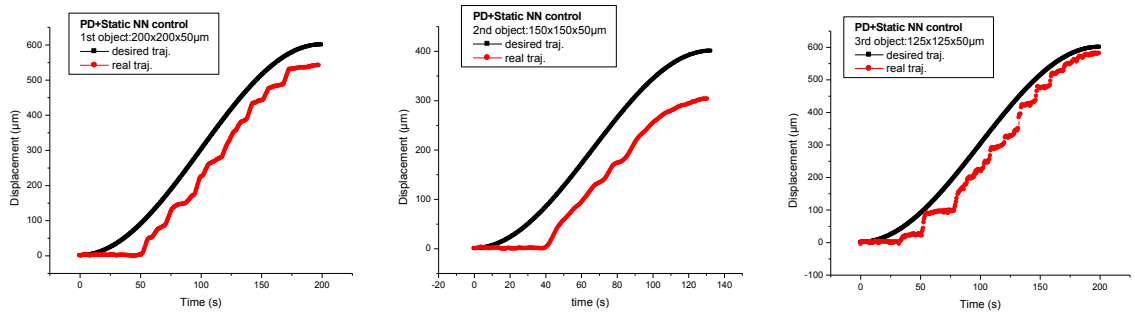

Figure 5-5. Actual trajectories of the micro objects in sequential micromanipulation by static NN-based controller (Run#2).

Adding the static NN does not produce any noticeable improvement of the overall performance of the automated sequential micromanipulation in Figure 5-5. This stems from the fact that the data used to train the NN does not truly represent the conditions under which the manipulation process takes place. The ambient condition in this run of the experiment differs from that of the training data sets. No micro forces characterization is performed on these specific micro objects used in the experiment in order to train the NN. This strategy is chosen to demonstrate the limitation of a non-adaptive control system for such micromanipulation where the governing forces are highly sensitive to any changes in the surface and ambient conditions.

5.8.3 Sequential Micromanipulation Using Proposed Adaptive NN-based Controller

The next five cycles of the automated sequential pushing are carried out by using the newly developed adaptive control system in which the W matrix is updated during the process according to (4.22) in the manner discussed in Section 5.7.1. Figure 5-6 represents the trajectories obtained in the second cycle of the experiment with the proposed adaptive NN-based controller. From these plots, it is evident that the controller is effectively adapting its parameter, progressively leading to an accurate positioning of the micro objects, based on the desired predefined trajectory.

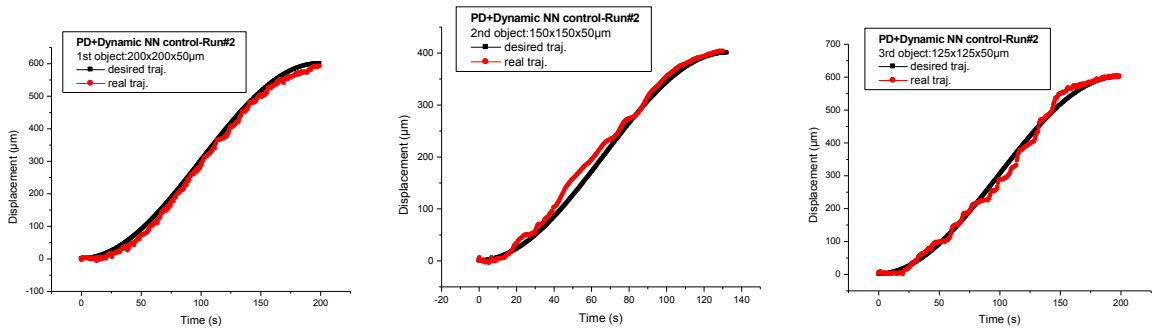

Figure 5-6. Actual trajectories of the micro objects in sequential micromanipulation by adaptive NN-based controller (Run#4).

To fine tune the controller parameters, the learning rate is decreased by half after the third cycle of the sequential micromanipulation is complete. Lowering the learning rate parameter implies taking smaller steps toward the "near" optimal values of the *W* matrix weights, thus, avoiding the problem of over tuning commonly encountered if the learning rate is larger than what is required after several epochs of training.

Fine tuning the adaptive controller results in an even more superior positioning of the micro objects. This can be seen from the plots in Figure 5-7. The three objects very closely follow the desired path.

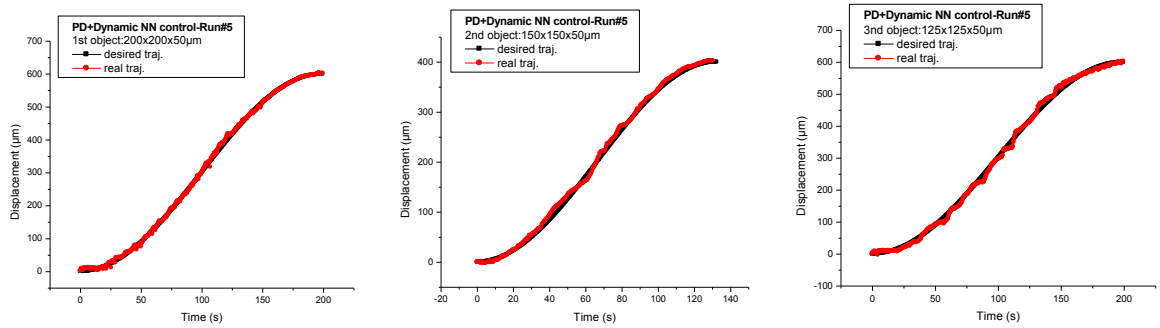

Figure 5-7. Actual trajectories of the micro objects in the sequential micromanipulation by adaptive NN-based controller (Run#7).

An example of the configuration of the micro objects before and after the automated sequential pushing is illustrated in Figure 5-8. As seen in this figure, the surface of the silicon substrate is not perfectly polished and contains a number of scratches. Despite this, the proposed adaptive controller learns how to correctly compensate for the micro forces at the different places on this substrate. The learning for

adapting to various characteristics of the surface asperities is facilitated by choosing the "position" of the object as a varying parameter in the input vector of the adaptive NN.

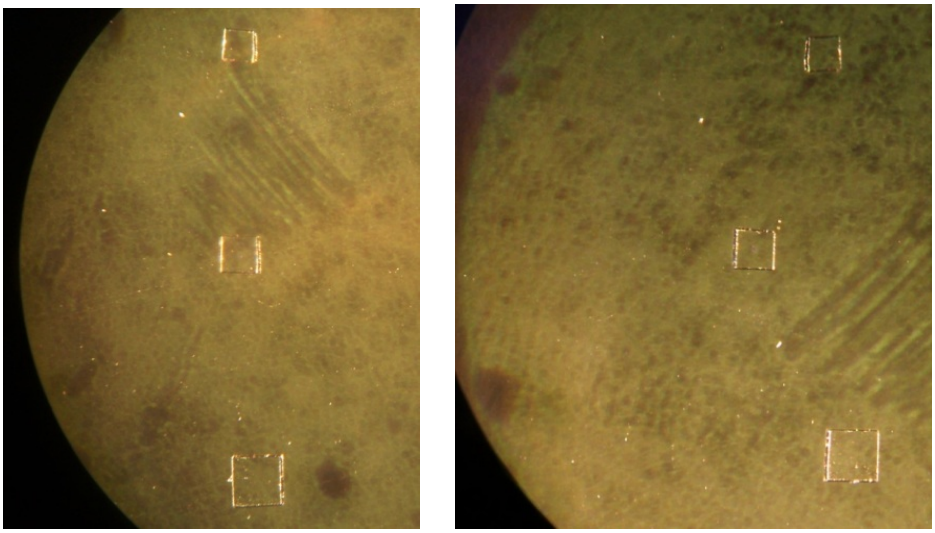

Figure 5-8. Position of micro objects before (left) and after (right) automated sequential pushing experiment (Note: the two pictures are taken from different experiments).

5.8.4 Numerical Analysis of the Results

The performance of the control system is evaluated by using the RMS of the errors over the course of the automated sequential micromanipulation. Equation (4.29) in Section 4.4.1 defines the RMS error for pushing a single object. In sequential micro pushing, the average RMS error is calculated as follows:

$$E_{RMS} = \frac{1}{3}(E_{RMS1} + E_{RMS2} + E_{RMS3}) \quad , \quad (5.5)$$

where $E_{RMS_i}$is the RMS calculated by using (4.29) for each individual pushing operation in the experiment of sequential pushing of the three objects. The results of these calculations are summarized in Table 5-3. Figure 5-9 compares the overall performance of the controller by plotting the average RMS error calculated in Table 5-3.

Table 5-3. Average RMS trajectory errors in automated sequential pushing experiment by different controller systems.

Run index	Controller	RMS_1	RMS_2	RMS_3	Average RMS
Run #1	PD only	54.35	121.84	79.01	85
Run #2	PD + static NN	66	75.93	53.50	65.14
Run #3	PD + dynamic NN	27.24	22.11	25.23	24.86
Run #4		15.67	14.32	16.30	15.43
Run #5		14.24	14.56	18.21	15.67
Run #6		5.23	7.22	7.24	6.56
Run #7		4.89	5.65	7.91	6.15

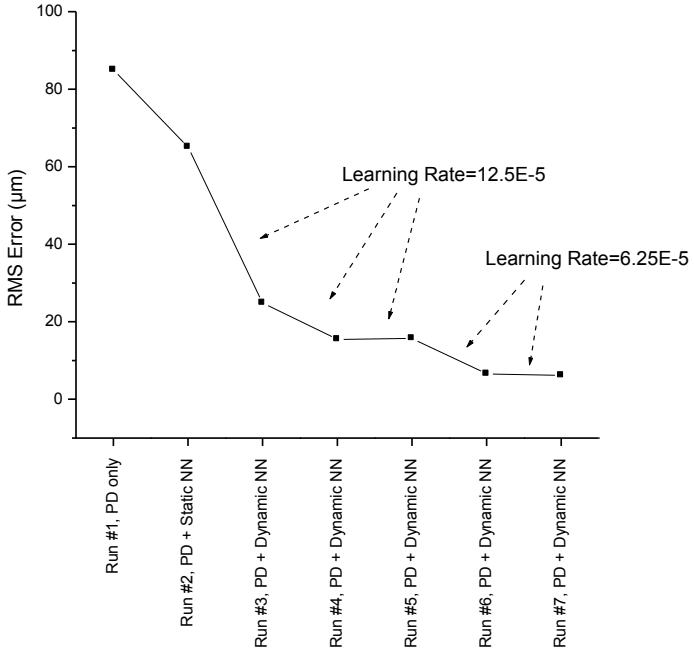

Figure 5-9. RMS trajectory errors at different runs of the automated sequential pushing experiments.

After several tests are completed and no significant change of the parameters affecting the micro forces are observed, the RMS curve typically hit a plateau at which the controller is no longer capable of learning more. At this point, the *W* matrix values undergo little or no updates, and the proposed adaptive NN is deemed to be trained satisfactorily. Any further decrease in the value of the learning rate has no significant effect in the average RMS. In this experiment, the adaptive controller performance does not improve beyond the fourth training cycle of the completed automated sequential pushing with the dynamic NN (Experiment Run#6).

Chapter 6
Discussion, Conclusion and Future Work

6.1 Discussion

This thesis is the first systematic study of the characterization of micro surface forces, present during the manipulation of micro size objects, specifically in pushing square micro objects with a large surface area on a flat surface. The limited resources in the literature on micro forces characterization is largely due to difficulties associated with sample preparation and system calibration. Preparing samples that are identical in their specifications and surface characterization, in terms of roughness, coating, surface chemistry, and contamination, are the most challenging aspects of micro force characterization.

A vast number of parameters affect the magnitude of micro forces. For conducting experiments for a successful characterization, only one of these parameters must be allowed to vary during a given pushing experiment. For example, if the effect of the temperature is investigated, the pushing experiments should always be conducted along a fixed line on the substrate to avoid the disturbances caused by the non-uniformity of substrate surface condition. If the object is pushed on different paths on the substrate, these disturbing factors make it difficult to determine the effect of the individual parameters under investigation.

In the absence of any analytical model for micro forces, the data reported in the micro forces characterization in this thesis, along with the inexpensive experimental setup, proposed for the micro forces measurement provides a platform for future experimental studies on the surface micro forces dominant in Micro Electro Mechanical Systems.

In addition, a nonlinear adaptive controller is designed to compensate for the effect of the micro forces. This controller is robust to the changes in any of the parameters in the sense that it takes only a few trials before the controller can learn to adapt the weights to the changes in these parameters. For example, the micro object size or the desired positioning trajectory on the substrate can be altered. In either scenario, the proposed six-input neural networks (NN) can be efficiently tuned in real time by repeatedly operating under the new conditions, provided that the parameters that are not included in the NN input vector remain static in the new value for the learning period.

Promising results, reported in the automated sequential manipulation, can promote the applicability of an adaptive NN in a precise manipulation in the micro scale under varying environmental conditions. In

serial automated microassembly lines, the dominant resisting micro forces distort the compliant micromanipulator tips, impairing the accuracy of the automated positioning. Micromanipulator systems with stiff arms do not have this issue; however, they have a very large physical footprint compared to that of the micro objects. This imposes a restriction on installing multiple manipulators to perform multi-degree-of-freedom (DOF) assembly tasks. The proposed compensation mechanism for micro forces enables the use of multiple miniaturized micromanipulators for the automated serial assembly of 3-D micro systems.

6.2 Conclusion

The specific contributions of this research can be summarized.

- The micro surface forces, dominant in pushing flat micro objects are investigated. An inexpensive vision-based experimental setup is designed and developed. It is capable of reliably measuring collective micro forces, and can replace expensive AFM for force characterization.
- The novel setup is tailored for conducting numerous experiments to establish some of the characteristics of surface micro forces. Similar to the friction in the macro world, static micro forces, kinetic micro forces, viscous micro forces, and stick-slip micro forces are characterized during micro object pushing.
- It is observed that due to the extremely high viscous micro forces at the velocities above a threshold, called the maximum achievable speed, micro objects never undergo a pushing speed above the threshold. This threshold is determined for different micro objects in different operational conditions in the range of 0.2μm/s to 5μm/s. According to the data in the experiments, flat micro object pushing on a flat substrate is an extremely slow process, resulting in a very low productivity of micromanipulators. This conclusion is reached by the definition of the scale speed and comparing its value in the micro object pushing process (0.002~0.03Hz) and macro object manipulation (100Hz).
- The effect of the temperature on the magnitude of the micro forces is examined. The resultant data suggest that, when the experimental environment is isolated from moisture, increasing the temperature results in decreasing the magnitude of the micro forces by 40% and increasing the maximum pushing speed by 400%. It is confirmed that these figures are consistent for various micro object sizes. The results substantially change, if moisture is introduced to the chamber to

keep the relative humidity constant in the environment. In another scenario, the temperature is kept constant, and the relative humidity is increased by adding more moisture to the environment. The graphs obtained in the last two scenarios suggest that the magnitude of the surface micro forces reflects a nonlinear relationship with the temperature and humidity.

- Also, it is demonstrated that the magnitude of the surface micro forces is linearly proportional to the area of contact.
- The substrate material is shown to have a significant impact on the moisture absorption based on their hydrophilicity, resulting in a substantial change in the magnitude of the micro forces.
- In the second part of this thesis, a controller is designed and implemented to compensate for the nonlinear micro forces. In the absence of any reliable model for various complex micro forces, an adaptive NN is proposed and incorporated in conjunction with a conventional PD controller. The stability of the proposed controller is proven in the sense of Lyapunov and a real time neural network weight update law is derived.
- The effectiveness of the proposed adaptive controller is verified in a series of micro object pushing experiments. The repeatability of the results presented in this work is also demonstrated.
- In this thesis, the automated sequential precise positioning of multiple micro objects is successfully realized. For the first time, the entire micromanipulation path is controlled by accurately compensating for the dominant micro forces involved.

6.3 Future Work

The following tasks are suggested for the continuation of this research.

- In the characterization, the effect of air pressure on micro forces should be considered. Air pressure affects the interaction between the surfaces of the objects and the environment. Consequently, it is worthwhile to investigate the effect of the atmospheric pressure on the magnitude of micro forces. There is also a plenty of room to investigate the effects of surface roughness as well as different materials on micro forces.

- The results obtained in this thesis reveal that pushing micro objects with a flat surface area on a flat substrate is a very slow process, when compared to manipulation of objects in macro scale. As illustrated in this thesis, the viscous micro forces in the process of pushing impose a substantial limitation to micromanipulation. Applications such as microassembly are prone to a low productivity, if flat micro objects are deemed to be pushed on flat substrates. Studies should be performed to explore innovative solutions to overcome the limitation, such as the selection of appropriate materials, roughening the surfaces, and conducting the operation at a specific ambient temperature, relative humidity, and air pressure.

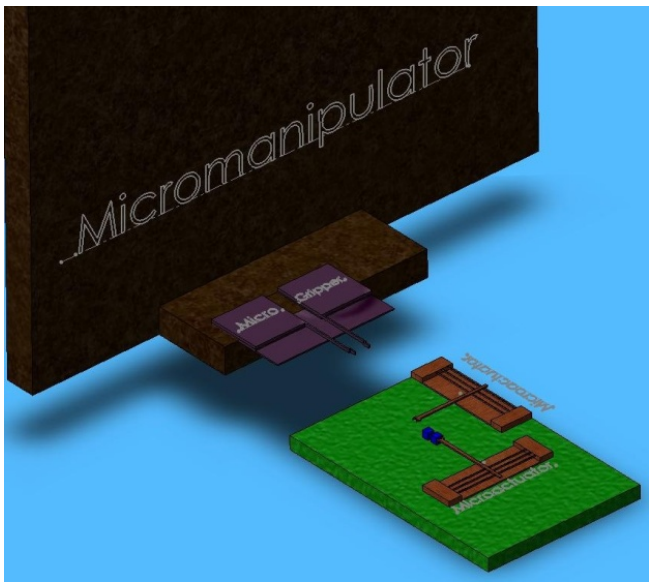

Figure 6-1. Schematic of the sequential microassembly of multiple micro components by microactuators.

- In this thesis, a slim micro cantilever with a high aspect ratio is employed. The deflection of the cantilever under a lateral load in the experiments closely simulates the effect of dominant micro forces on compliant microactuators. For future work, the proposed adaptive controller can be implemented to command multi DOF microactuators for accurately positioning micro objects. Figure 6-1 illustrates different micro components that are sequentially pushed by two microactuators in xy plane to the pick-up station by a microgripoper. The proposed controller can be applied to each of these one DOF microactuators.

- Moreover, once a reliable multi DOF microactuator is realized, the proposed controller can be extended from a single-output to multi-outputs. Such a controller can then be implemented to control all the linkages of the multi DOF microactuator.
- Biomedical labs will benefit significantly if cell positioning and various post-processing tasks, such as the microinjection of foreign molecules, in vitro fertilization, and directed stem cell differentiation can be automatically performed on a single cell sequentially. These cell manipulation operations can be realized with a high yield, improved cell viability, and high throughput by operating multiple miniaturized micromanipulators which are controlled robustly by using the proposed adaptive controller. The development of appropriate micromanipulators that are biocompatible with the cell manipulation environment is necessary before the proposed controller can be extended to the biomedical applications.

Bibliography

1. Dechev, N., Cleghorn, W.L., and Mills, J.K., *Microassembly of 3-D microstructures using a compliant, passive microgripper.* Journal of Microelectromechanical Systems, 2004. **13**(2): p. 176-189.

2. Wang, L.D., Mills, J.K., and Cleghorn, W.L., *Novel approach for microassembly of three-dimensional rotary MOEMS mirrors.* Journal of Micro-Nanolithography Mems and Moems, 2009. **8**(4).

3. Dechev, N., Basha, M., Chaudhuri, S.K., and Safavi-Naeini, S., *Microassembly of 3D micro-mirrors as building elements for optical MEMS switching*, in *Optomechatronic Micro/Nano Devices and Components II*. 2006. p. 111-122.

4. Chen, L.G., Chen, T., Sun, L.N., and Rong, W.B., *Automatic microassembly system for die level fabrication of MEMS pressure sensor.* Iciea 2007: 2nd Ieee Conference on Industrial Electronics and Applications, Vols 1-4, Proceedings, 2007: p. 1079-1083

5. Yao, Y., Gulari, M.N., Wiler, J.A., and Wise, K.D., *A microassembled low-profile three-dimensional microelectrode array for neural prosthesis applications.* Journal of Microelectromechanical Systems, 2007. **16**(4): p. 977-988.

6. Maier, S.A., Kik, P.G., Atwater, H.A., Meltzer, S., Harel, E., Koel, B.E., and Requicha, A.A.G., *Local detection of electromagnetic energy transport below the diffraction limit in metal nanoparticle plasmon waveguides.* Nature Materials, 2003. **2**(4): p. 229-232.

7. Tafazzoli, A., Cheng, C.M., Pawashe, C., Sabo, E.K., Trofin, L., Sitti, M., and Leduc, P.R., *Subfeature patterning of organic and inorganic materials using robotic assembly.* Journal of Materials Research, 2007. **22**(6): p. 1601-1608.

8. Carlsson, S.B., Junno, T., Montelius, L., and Samuelson, L., *Mechanical tuning of tunnel gaps for the assembly of single-electron transistors.* Applied Physics Letters, 1999. **75**(10): p. 1461-1463.

9. Lu, J.H., *Nanomanipulation of extended single-DNA molecules on modified mica surfaces using the atomic force microscopy.* Colloids and Surfaces B-Biointerfaces, 2004. **39**(4): p. 177-180.

10. Lu, Z., Moraes, C., Zhao, Y., You, L.D., Simmons, C.A., and Sun, Y., *A Micromanipulation System for Single Cell Deposition.* 2010 Ieee International Conference on Robotics and Automation (Icra), 2010: p. 494-499.

11. Basha, M.A., Dechev, N., Safavi-Naeini, S., and Chaudhuri, S.K., *Improved design of large 3-D micromirrors for microassembly into an optical MEMS cross-connect.* Optomechatronic Micro/Nano Devices and Components III, 2007. **6717**: p. 71701-71701.

12. Gorman, J.J., Dagalakis, N.G., and Boone, B.G., *Multi-loop control of a nanopositioning mechanism for ultra-precision beam steering.* Free-Space Laser Communication and Active Laser Illumination, 2004. **5160**: p. 170-181.

13. Cavalcanti, A., Shirinzadeh, B., Freitas, R.A., and Hogg, T., *Nanorobot architecture for medical target identification.* Nanotechnology, 2008. **19**(1).

14. Brenan, C.J.H., Doukoglou, T.D., Hunter, I.W., and Lafontaine, S., *Characterization and Use of a Novel Optical Position Sensor for Microposition Control of a Linear Motor.* Review of Scientific Instruments, 1993. **64**(2): p. 349-356.

15. Freitas, R.A., *The Future of Nanomedicine.* Futurist, 2010. **44**(1): p. 21-22.

16. Asano, H., Qiu, Z.J., Zhou, L.B., Ojima, H., Shimizu, J., Ishikawa, T., and Edal, H., *Path control scheme for vision guided micro manipulation system.* Towards Synthesis of Micro -/Nano - Systems, 2007(5): p. 321-322.

17. Sun, Y. and Nelson, B.J., *Biological cell injection using an autonomous microrobotic system.* International Journal of Robotics Research, 2002. **21**(10-11): p. 861-868.

18. Cavalcanti, A., Rosen, L., Kretly, L.C., Rosenfeld, M., and Einav, S., *Nanorobotic challenges in biomedical applications, design and control.* ICECS 2004: 11th IEEE International Conference on Electronics, Circuits and Systems, 2004: p. 447-450.

19. Hunter, I.W., Jones, L.A., Sagar, M.A., Lafontaine, S.R., and Hunter, P.J., *Ophthalmic Microsurgical Robot and Associated Virtual Environment.* Computers in Biology and Medicine, 1995. **25**(2): p. 173-177.

20. Elbuken, C., Gui, L., Ren, C.L., Yavuz, M., and Khamesee, M.B., *Design and Characterization of a Polymeric Photo Thermal Microgripper for Micromanipulation.* Proceedings of the Asme International Mechanical Engineering Congress and Exposition, Vol 13, Pts a and B, 2009: p. 521-527.

21. Verma, S., Kim, W.J., and Gu, J., *Six-axis nanopositioning device with precision magnetic levitation technology.* Ieee-Asme Transactions on Mechatronics, 2004. **9**(2): p. 384-391.

22. Ye, X.Y., Huang, Y., Zhou, Z.Y., Li, Q.C., and Gong, Q.L., *A magnetic levitation actuator for micro-assembly.* Transducers 97 - 1997 International Conference on Solid-State Sensors and Actuators, Digest of Technical Papers, Vols 1 and 2, 1997: p. 797-799.

23. Sinan Haliyo D, D.F., Regnier S *Controlled rolling of microobjects for autonomous manipulation.* Journal of Micromechatronics 2006(3): p. 75-101.

24. Arai, F. and Fukuda, T., *Adhesion-type micro endeffector for micromanipulation.* 1997 Ieee International Conference on Robotics and Automation - Proceedings, Vols 1-4, 1997: p. 1472-1477.

25. Toset, J., Casuso, I., Samitier, J., and Gomila, G., *Deflection-voltage curve modelling in atomic force microscopy and its use in DC electrostatic manipulation of gold nanoparticles.* Nanotechnology, 2007. **18**(1).

26. Thompson, J.A. and Fearing, R.S., *Automating microassembly with ortho-tweezers and force sensing.* Iros 2001: Proceedings of the 2001 Ieee/Rjs International Conference on Intelligent Robots and Systems, Vols 1-4, 2001: p. 1327-1334.

27. Zhou, Q., Chang, B., and Koivo, H.N., *Temperature and humidity effects on micro/nano handling.* Advances in Materials Manufacturing Science and Technology II, 2006. **532-533**: p. 681-684.

28. Chan, H.Y. and Li, W.J., *Design and fabrication of a micro thermal actuator for cellular grasping.* Acta Mechanica Sinica, 2004. **20**(2): p. 132-139.

29. Neild, A., Oberti, S., Beyeler, F., Dual, J., and Nelson, B.J., *A micro-particle positioning technique combining an ultrasonic manipulator and a microgripper.* Journal of Micromechanics and Microengineering, 2006. **16**(8): p. 1562-1570.

30. Chang, W.C., Lee, L.P., and Liepmann, D., *Adhesion-based capture and separation of cells for microfluidic devices.* Biomems and Bionanotechnology, 2002. **729**: p. 155-160.

31. Sitti, M., *Atomic force microscope probe based controlled pushing for nanotribological characterization.* Ieee-Asme Transactions on Mechatronics, 2004. **9**(2): p. 343-349.

32. Cappella, B. and Dietler, G., *Force-distance curves by atomic force microscopy.* Surface Science Reports, 1999. **34**(1-3).

33. Last, M., Subramaniam, V., and Pister, K.S.J., *Out of plane motion of assembled microstructures using a single-mask SOI process.* Transducers '05, Digest of Technical Papers, Vols 1 and 2, 2005: p. 684-687.

34. Bohringer, K.F., Goldberg, K., Cohn, M., Howe, R., and Pisano, A., *Parallel microassembly with electrostatic force fields.* 1998 Ieee International Conference on Robotics and Automation, Vols 1-4, 1998: p. 1204-1211.

35. Nakao, M., Kazuhisa, I., Tomomasa, S., and Yotaro, H., *Test of nontweezing micro handling tools with releasing mechanism/prototypes of mirco nontweezing handling tools with releasing mechanism.* Jpn Mach Acad Soc J C, 1995. **61**(583): p. 1021-6.

36. Chen, S.C., Culpepper, M.L., and Jordan, S., *Six-axis compliant mechanisms for manipulation of micro-scale fiber optics components - art. no. 64660P.* MOEMS and Miniaturized Systems VI, 2007. **6466**: p. 4660-4660.

37. Gauthier, M. and Piat, E., *Control of a particular micro-macro positioning system applied to cell micromanipulation.* Ieee Transactions on Automation Science and Engineering, 2006. **3**(3): p. 264-271.

38. Shen, Y.T., Xi, N., Wejinya, U.C., Li, W.J., and Xiao, J.H., *Infinite dimension system approach for hybrid force/position control in micromanipulation.* 2004 Ieee International Conference on Robotics and Automation, Vols 1- 5, Proceedings, 2004: p. 2912-2917.

39. Beyeler, F., Neild, A., Oberti, S., Bell, D.J., Sun, Y., Dual, J., and Nelson, B.J., *Monolithically fabricated microgripper with integrated force sensor for manipulating microobjects and biological cells aligned in an ultrasonic field.* Journal of Microelectromechanical Systems, 2007. **16**(1): p. 7-15.

40. Wason, J., Gressick, W., Wen, J.T., Gorman, J., and Dagalakis, N., *Multi-probe micro-assembly.* 2007 Ieee International Conference on Automation Science and Engineering, Vols 1-3, 2007: p. 886-891.

41. Shen, J., Xi, J.Y., Zhu, W.T., Chen, L.Q., and Qiu, X.P., *A nanocomposite proton exchange membrane based on PVDF, poly(2-acrylamido-2-methyl propylene sulfonic acid), and nano-Al2O3 for direct methanol fuel cells.* Journal of Power Sources, 2006. **159**(2): p. 894-899.

42. Attard, P., *Friction, adhesion, and deformation: dynamic measurements with the atomic force microscope.* Journal of Adhesion Science and Technology, 2002. **16**(7): p. 753-791.

43. Mokaberi, B., Yuri, J.C., Wang, M., and Requicha, A.A.G., *Automated nanomanipulation with atomic force microscopes.* Proceedings of the 2007 Ieee International Conference on Robotics and Automation, Vols 1-10, 2007: p. 1406-1412.

44. Shen, Y.T., Xi, N., Li, W.J., and Wang, Y.X., *Dynamic performance enhancement of PVDF force sensor for micromanipulation.* 2005 IEEE/RSJ International Conference on Intelligent Robots and Systems, Vols 1-4, 2005: p. 1172-1177.

45. Lopez, D., Decca, R.S., Fischbach, E., and Krause, D.E., *MEMS-based force sensor: Design and applications.* Bell Labs Technical Journal, 2005. **10**(3): p. 61-80.

46. Sun, Y., Nelson, B.J., Potasek, D.P., and Enikov, E., *A bulk microfabricated multi-axis capacitive cellular force sensor using transverse comb drives.* Journal of Micromechanics and Microengineering, 2002. **12**(6): p. 832-840.

47. Jeong, K.H., Keller, C.G., and Lee, L.P., *Direct force measurements of biomolecular interactions by nanomechanical force gauge.* Applied Physics Letters, 2005. **86**(19).

48. Yantao Shen and Xi, N., *Networked human/robot cooperative environment for teleassembly of MEMS devices,".* J of micromechatronics, 2006. **3**(3): p. 239-266.

49. Chen, H.P., Xi, N., and Li, G.Y., *CAD-guided automated nanoassembly using atomic force microscopy-based nonrobotics.* Ieee Transactions on Automation Science and Engineering, 2006. **3**(3): p. 208-217.

50. Sun, Y., Greminger, M.A., and Nelson, B.J., *Nanopositioning of a multi-axis microactuator using visual servoing,".* J. of Micromechatronics, 2004. **2**(2): p. 141-155.

51. Deladi, S., Krijnen, G., and Elwenspoek, M.C., *Parallel-beams/lever electrothermal out-of-plane actuator.* Microsystem Technologies-Micro-and Nanosystems-Information Storage and Processing Systems, 2004. **10**(5): p. 393-399.

52. Xie, H.K. and Fedder, G.K., *Vertical comb-finger capacitive actuation and sensing for CMOS-MEMS.* Sensors and Actuators a-Physical, 2002. **95**(2-3): p. 212-221.

53. Braun, K.M., Niemann, C., Jensen, U.B., Sundberg, J.P., Silva-Vargas, V., and Watt, F.M., *Manipulation of stem cell proliferation and lineage commitment: visualisation of label-retaining cells in wholemounts of mouse epidermis.* Development, 2003. **130**(21): p. 5241-5255.

54. Chen, S.C. and Culpepper, M.L., *Design of a six-axis micro-scale nanopositioner - mu HexFlex.* Precision Engineering-Journal of the International Societies for Precision Engineering and Nanotechnology, 2006. **30**(3): p. 314-324.

55. Tung, Y.C. and Kurabayashi, K., *A single-layer multiple degree-of-freedom PDMS-on-silicon dynamic focus micro-lens.* MEMS 2006: 19th IEEE International Conference on Micro Electro Mechanical Systems, Technical Digest, 2006: p. 838-841

56. Hollar, S., Flynn, A., Bellew, C., and Pister, K.S.J., *Solar powered 10 mg silicon robot.* Mems-03: Ieee the Sixteenth Annual International Conference on Micro Electro Mechanical Systems, 2003: p. 706-711.

57. Cohn, M.B., Bohringer, K.F., Noworolski, J.M., Singh, A., Keller, C.G., Goldberg, K.Y., and Howe, R.T., *Microassembly technologies for MEMS.* Materials and Device Characterization in Micromachining, 1998. **3512**: p. 2-16.

58. Hung, A.M. and Stupp, S.I., *Simultaneous self-assembly, orientation, and patterning of peptide-amphiphile nanofibers by soft lithography.* Nano Letters, 2007. **7**(5): p. 1165-1171.

59. Xiong, X.R., Hanein, Y., Fang, J.D., Wang, Y.B., Wang, W.H., Schwartz, D.T., and Bohringer, K.F., *Controlled multibatch self-assembly of microdevices.* Journal of Microelectromechanical Systems, 2003. **12**(2): p. 117-127.

60. Bohringer, K.F., *Surface modification and modulation in microstructures: controlling protein adsorption, monolayer desorption and micro-self-assembly.* Journal of Micromechanics and Microengineering, 2003. **13**(4): p. S1-S10.

61. Zhou, Q. and Chang, B., *Microhandling using robotic manipulation and capillary self-alignment.* 2006 IEEE/RSJ International Conference on Intelligent Robots and Systems, Vols 1-12, 2006: p. 5883-5888.

62. Tsang, S.H., Sameoto, D., Foulds, I.G., Johnstone, R.W., and Parameswaran, M., *Automated assembly of hingeless 90 degrees out-of-plane microstructures.* Journal of Micromechanics and Microengineering, 2007. **17**(7): p. 1314-1325.

63. Lai, K.W.C. and Li, W.J., *Automated Micro-Assembly of MOEMS by Centrifugal Force*, in *IEEE/ASME M2VIP*. 2002: Chang Mai, Thailand.

64. Feddema, J.T. and Christenson, T.R., *Parallel assembly of high aspect ratio microstructures.* Microrobotics and Microassembly, 1999. **3834**: p. 153-164.

65. Heinz, W. *From decimeter- to centimeter-sized mobile microrobots - The development of the MINIMAN system*. in *The International Society for Optical Engineering*. 2001.

66. Buerkle, A., Schmoeckel, F., Kiefer, M., Amavasai, B.P., Caparrelli, F., Selvan, A.N., and Travis, J.R., *Vision-based closed-loop control of mobile microrobots for micro handling tasks.* Microrobotics and Microassembly Iii, 2001. **4568**: p. 187-198.

67. Edqvist, E., Snis, N., Sjolund, M., Murase, T., Soderberg, A., and Johansson, S., *The Assembly of Millimeter Sized Mass Producible Autonomous Robots.* Actuator 08, Conference Proceedings, 2008: p. 304-307.

68. Kim, S., Knoll, T., and Scholz, O., *Feasibility of inductive communication between millimeter-sized robots.* 2006 1st IEEE RAS-EMBS International Conference on Biomedical Robotics and Biomechatronics, Vols 1-3, 2006: p. 165-169.

69. Delrio, F.W., De Boer, M.P., Knapp, J.A., Reedy, E.D., Clews, P.J., and Dunn, M.L., *The role of van der Waals forces in adhesion of micromachined surfaces.* Nature Materials, 2005. **4**(8): p. 629-634.

70. Mo, Y.F., Turner, K.T., and Szlufarska, I., *Friction laws at the nanoscale.* Nature, 2009. **457**(7233): p. 1116-1119.

71. Armstronghelouvry, B., *A Survey of Models, Analysis Tools and Compensation Methods for the Control of Machines with Friction.* Automatica, 1994. **30**(7): p. 1083-1138.

72. Chung, D.W. and Yang, S.H., *Stick-slip friction compensation for mechatronic servo systems.* Proceedings of the 23rd IASTED International Conference on Modelling, Identification, and Control, 2004: p. 611-615.

73. Lumbantobing, A. and Komvopoulos, K., *Static friction in polysilicon surface micromachines.* Journal of Microelectromechanical Systems, 2005. **14**(4): p. 651-663.

74. Wu, J.H., Zhao, G., and Chu, J.R., *Influences of environmental humidity on micro object handling efficiency.* Journal of Micromechanics and Microengineering, 2007. **17**(2): p. 187-192.

75. Deng, K., Ko, W.H., and Michal, G.M., *A preliminary study on friction measurement in MEMS* Transducers 1991. **91**: p. 213-216.

76. Tas, N.R., Gui, C., and Elwenspoek, M., *Static friction in elastic adhesion contacts in MEMS.* Journal of Adhesion Science and Technology, 2003. **17**(4): p. 547-561.

77. Greenwoo.Ja and Williams.Jb, *Contact of Nominally Flat Surfaces.* Proceedings of the Royal Society of London Series a-Mathematical and Physical Sciences, 1966. **295**(1442): p. 300-303.

78. Crassous, J., Charlaix, E., Gayvallet, H., and Loubet, J.L., *Experimental-Study of a Nanometric Liquid Bridge with a Surface Force Apparatus.* Langmuir, 1993. **9**(8): p. 1995-1998.

79. Feddema, J.T., Xavier, P., and Brown, R., *Micro-assembly planning with van der Waals force* in *IEEE Int. Symp. On Assembly and Task Plans* 1999: Porto, Portugal. p. 32-38.

80. Bevan, M.A. and Prieve, D.C., *Direct measurement of retarded van der Waals attraction.* Langmuir, 1999. **15**(23): p. 7925-7936.

81. Lewis, F.L., Jagannathan, S., and Yesildirek, A., *Neural Network Control of Robot Manipulators and Nonlinear Systems*. 1998 London: Taylor & Fracis.

82. Haykin, S., *Neural Network: A Comprehensive Foundation* 1999, Upper Saddle River, NJ: Prentice Hall.

83. Chen, T.P., Chen, H., and Liu, R.W., *Approximation Capability in C((R)over-Bar(N)) by Multilayer Feedforward Networks and Related Problems.* Ieee Transactions on Neural Networks, 1995. **6**(1): p. 25-30.

84. Hornik, K., Stinchcombe, M., and White, H., *Multilayer Feedforward Networks Are Universal Approximators.* Neural Networks, 1989. **2**(5): p. 359-366.

85. ASME, *Surface Texture Symbols*. 1996.

86. Yang, Q.M. and Jagannathan, S., *A suite of robust controllers for the manipulation of microscale objects.* Ieee Transactions on Systems Man and Cybernetics Part B-Cybernetics, 2008. **38**(1): p. 113-125.

87. Natural History Magazine, March 1974, The American Museum of Natural History; James G. Doherty, general curator, The Wildlife Conservation Society

88. Shelby Supercars' press release, “http://www.shelbysupercars.com/press.php” {last retrieved in Feb 2010}

89. UIM Yearbook 2008/2009, Union Internationale Motonautique, 2009.

90. General Aviation World Records, Fédération Aéronautique Internationale, “http://records.fai.org/general_aviation/absolute.asp”,{ last retrieved in Feb 2010}